1967

Shape induced biaxial anisotropy in thin magnetic films

Fred Shing-Chung Lee
Iowa State University

SHAPE INDUCED BIAXIAL ANISOTROPY IN THIN MAGNETIC FILMS

by

Fred Shing-Chung Lee

A Dissertation Submitted to the
Graduate Faculty in Partial Fulfillment of
The Requirements for the Degree of
DOCTOR OF PHILOSOPHY

Major Subject: Electrical Engineering

Approved:

Signature was redacted for privacy.

In Charge of Major Work

Signature was redacted for privacy.

Head of Major Department

Signature was redacted for privacy.

Dean of Graduate College

Iowa State University
Of Science and Technology
Ames, Iowa

1967

TABLE OF CONTENTS

I. INTRODUCTION

A. The Problem

The purpose of this investigation was to study the relationship between shape induced biaxial anisotropy and the geometrical shape of a thin magnetic film element. Furthermore, an analytical expression relating biaxial anisotropy and the shape of an element was developed so as to provide a guide for the design of a biaxial memory element.

Because biaxial anisotropy as experimentally verified is induced by the geometrical shape effect of a film, and the shape of the film only influences the demagnetizing field distributions inside the film, it is reasonable to assume that the biaxial anisotropy comes strictly from the demagnetizing energy of the film element. From the experimental results as well as the numerical calculations, it is found that for a fixed orienting field a star-shaped film as indicated in Figure 1 has the highest magnetic energy when the average magnetization is in the 90° position (see Figure 2), and the lowest energy when the average magnetization is in the 45° position (see Figure 4). The corresponding orientational distributions of magnetization are shown in Figures 3 and 5. This energy difference (between the highest and the lowest energies) can be attributed to the biaxial property of the film.

To solve the continuous distribution of magnetization and hence the demagnetizing field in a thin magnetic film constitutes a nonlinear minimization problem. For theoretical interest, a general formulation for the two dimensional case has been derived in chapter II and it yields a total of 15 simultaneous partial differential equations. To solve

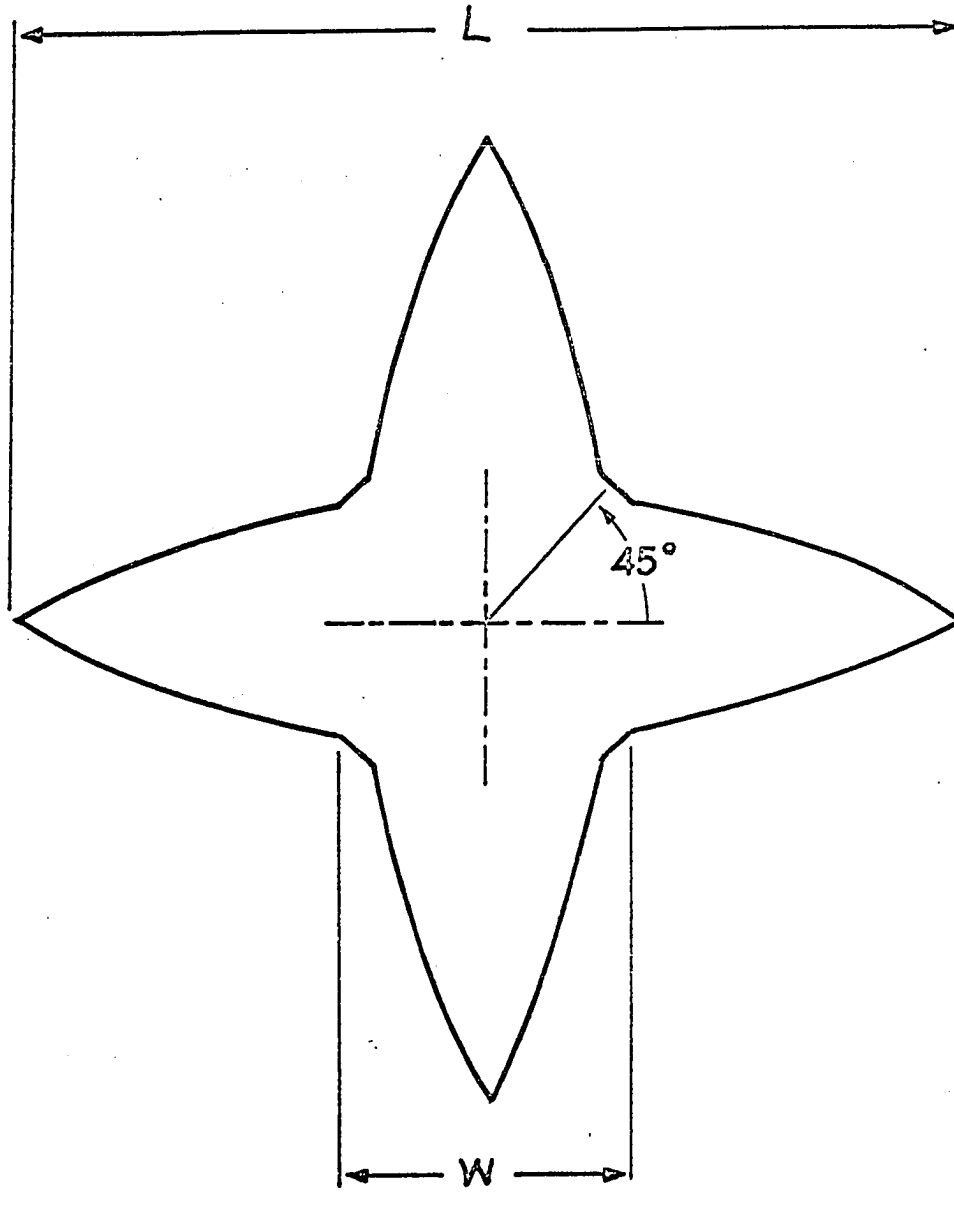

Figure 1. Star-shaped film element

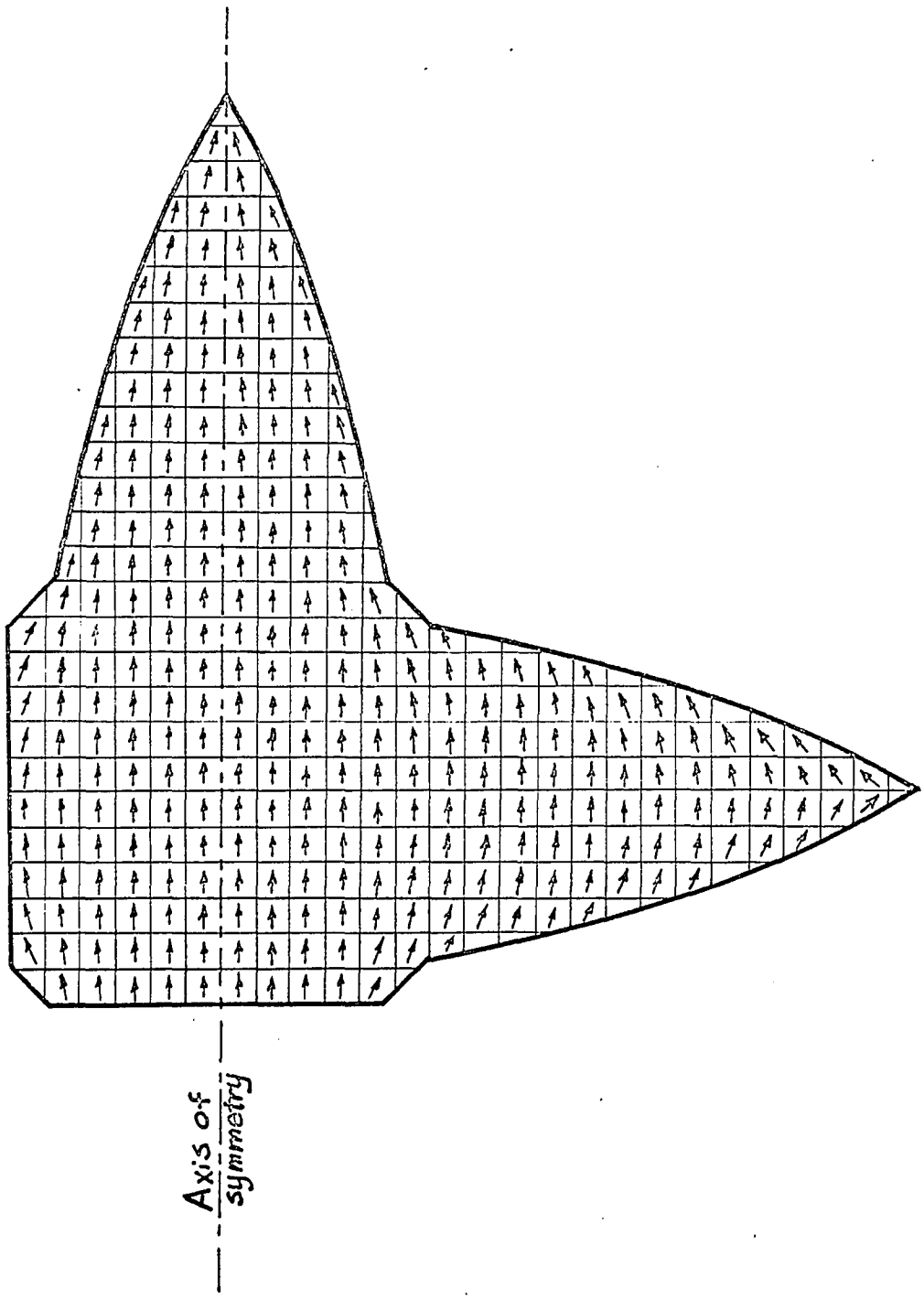

Figure 2. 90° M-distribution

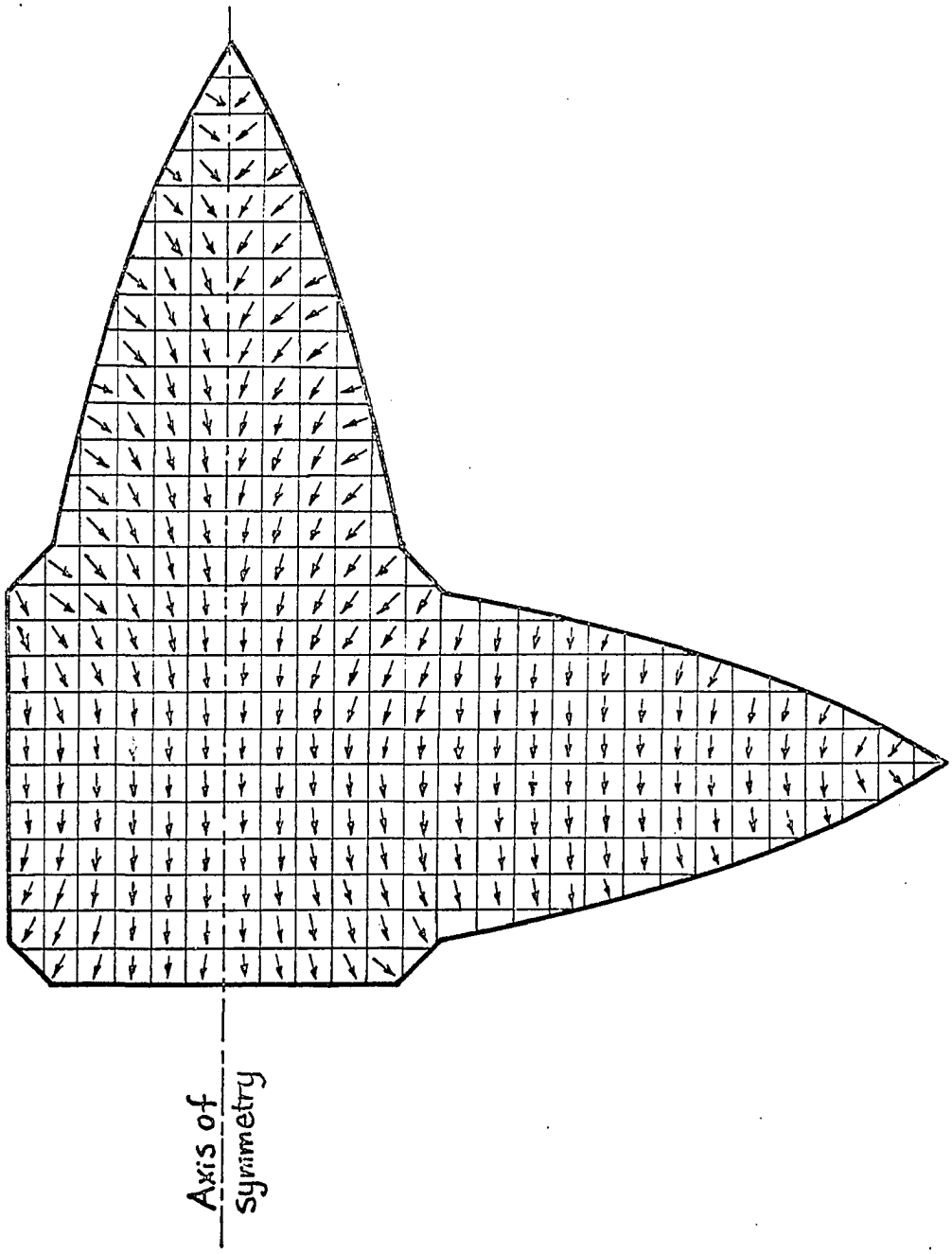

Figure 3. Orientations of demagnetizing fields due to 90° M-distribution

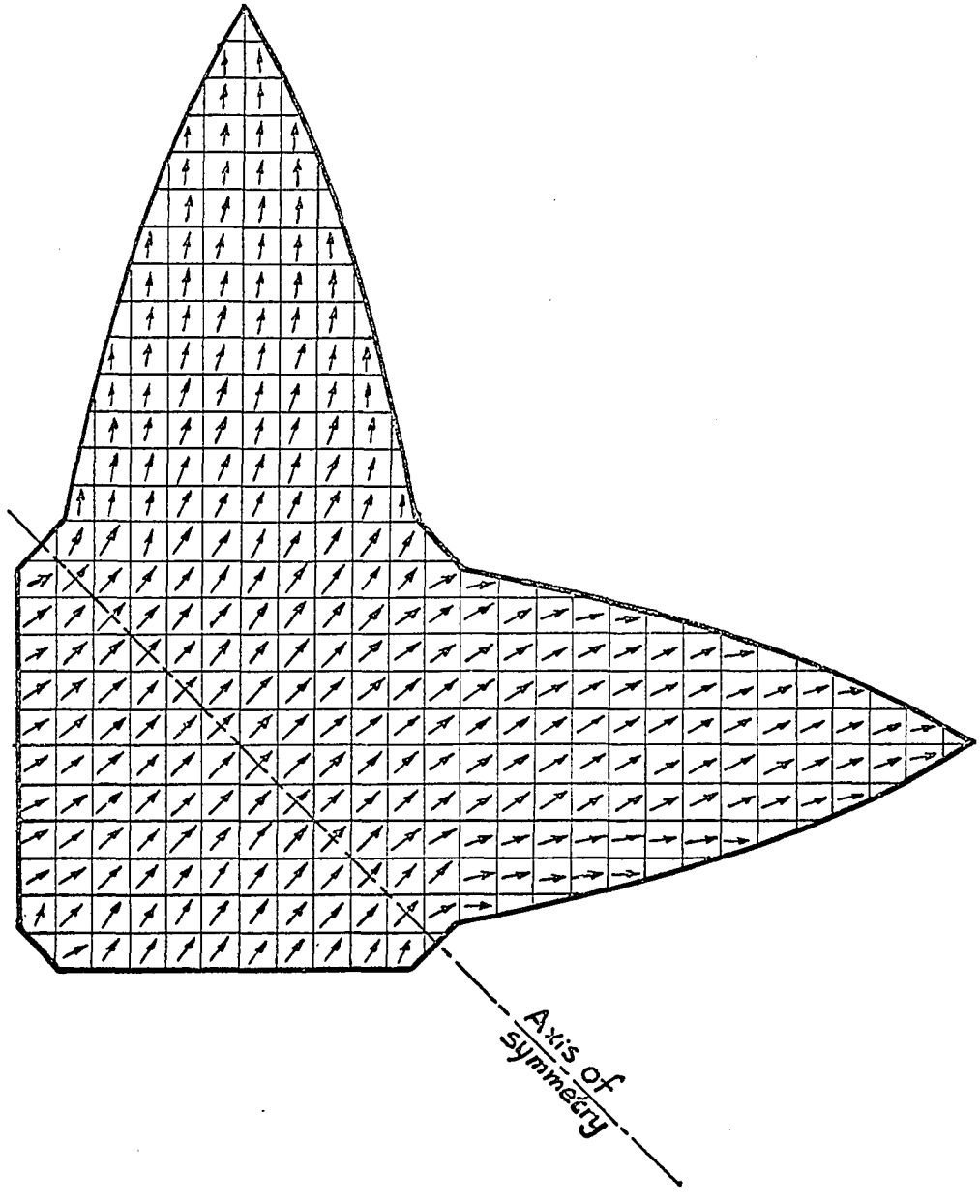

Figure 4. 45° M-distribution

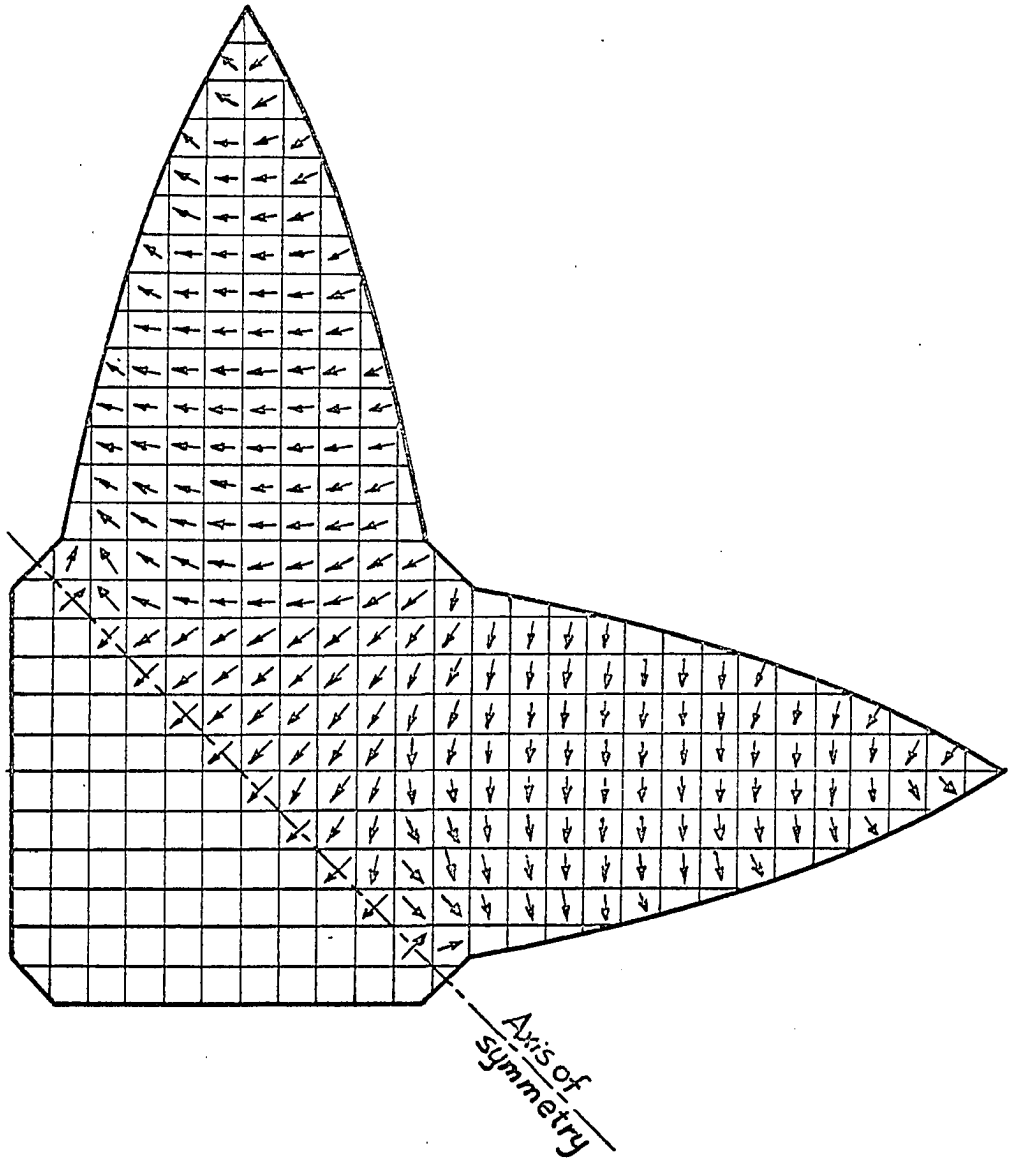

Figure 5. Orientations of demagnetizing fields due to 45° M-distribution

these equations becomes an extremely complicated task itself. So it is not considered further.

According to Brown (1) an arbitrary single-domain particle with uniform magnetization in a uniform applied field behaves like a suitably chosen ellipsoid of the same volume. Thus the magnetic energy of the star-shaped film would be independent of the orientation of the magnetization if the latter is assumed to be uniform. In order to have different magnetic energies for different orientations of magnetization, it is necessary to assume a non-uniform distribution of magnetization throughout the film.

In the numerical calculation which is used in this investigation, the film is divided into square partitions (40 divisions from tip to tip) in each of which the magnetization is assumed to be uniform. Any discontinuity of orientations of magnetization between neighboring partitions shows up as a surface magnetic charge density on the interfaces between these partitions. The demagnetizing field at the center of each of the partitions is calculated according to this magnetic charge distribution. A new orientation of magnetization in each of these partitions is then obtained under the minimum energy conditions in presence of the demagnetizing field and an orienting field. The final discrete and quasi-equilibrium distribution of magnetization throughout the film is obtained by an iterative process. The total magnetic energy for this particular distribution of magnetization is simply the summation of the scalar product of the vector magnetization and the demagnetizing field in each of the partitions. Note that the orienting field has been entered as one of

the parameters in calculating the equilibrium angles of magnetization; thus the biaxial anisotropy described here becomes dependent on the orienting field. It has been observed both theoretically and experimentally that this biaxial anisotropy decreases as the magnitude of the applied orienting field increases. Uniformly distributed magnetization is a special case which is theoretically equivalent to an infinite orienting field. The numerical calculation yields for this case a biaxial anisotropy of negligible value.

B. Review of Literature

Biaxial anisotropy in magnetic films from different origins have been reported by several authors, namely single-crystal films (2), scratched films (3) and double-layer films (4).

Thin single-crystal films of various ferromagnetic materials such as Ni, Fe, Ni-Fe and Ni-Co can be grown epitaxially by vacuum deposition onto heated rock salt. The deposited films assume a single-crystal structure with the same orientation as that of the substrate. This is due to an atomic interaction between the substrate and the deposited atoms. The biaxial anisotropy in this type of film is derived from the crystalline anisotropy which can be described simply in the following manner (5):

$$E_a = K_2(\alpha_1^2\alpha_2^2 + \alpha_2^2\alpha_3^2 + \alpha_3^2\alpha_1^2) + K_3(\alpha_1^2\alpha_2^2\alpha_3^2)$$

where K_2 and K_3 are material dependent constants and the $\alpha_{i's}$ are direction cosines with three crystalline axes. For a thin film such that $\alpha_3 = 0$ and with the magnetization vector lying entirely in the plane of the film, this energy can be reduced to

$$E_a = K_2(\alpha_1^2\alpha_2^2) \ .$$

If ϕ is the angle measured from the easy axis of the film, it may further simplify as

$$E_a = \frac{1}{4} K_2 \sin^2 2\phi \ .$$

This is the biaxial anisotropy contribution to the magnetic energy of the film.

The preparations and measured values of crystalline biaxial anisotropy of various ferromagnetic alloy films are given by Boyd (2). A study of magnetic switching in Ni-Fe single-crystal films has been made by Lo and Torok (6), in which they have compared hysteresis loops and switching critical curves both theoretically and experimentally. However, their experimental results show that due to large inhomogeneity in the anisotropy field in their samples, their particular films will not function as memory elements in the way originally proposed for an ideal biaxial film (5). A further extensive study of the magnetic switching in Ni-Fe single-crystal films with the aid of the Lorentz microscopy techniques was made by Lo (7), in which the Lorentz micrographs show the detailed switching process for two types of single-crystal Ni-Fe films at different reversal field angles as well as a theoretical explanation of different kinds of switching. Experimental results show that even the nearly perfect Ni-Fe single-crystal films do not switch coherently as a single-domain. The switching processes are different for two different types of single-crystal films and for different reversal field orientations. So far the difficulties in preparation of single-crystal film make it less attractive for

practical applications.

The biaxial anisotropy of scratched films (3) is attributed to a shape effect resulting from fine structure of the scratches on glass substrate. The orientation of the easy axis is always 45° to the scratch. The magnitude of the biaxial anisotropy constant increases with increasing roughness of scratches and is proportional to the square of the saturation magnetization. It is also field dependent since it decreases with increasing measuring field. A maximum biaxial anisotropy constant of 4.7×10^{4} ergs/cm^3 has been observed at a measuring field of 500 Oe. The scratches on the substrate are a composite of rectangularly shaped, tiny pits laid end to end. The film deposited on such a glass substrate is thus an array of oriented rectangular areas with dimensions of 18 x 18 μ in area and 0.8 μ in thickness and a separation from each other of 7.0 μ. The easy axes are along the diagonals of the squares. The usual uniaxial anisotropy constant of the scratched film is very small compared with the biaxial term. The disadvantage of inducing biaxial anisotropy in this way is the difficulty in control of the uniformity and reproducibility of the scratches which have definite effect on the magnitude of this very biaxial property.

Another source of biaxial anisotropy in thin magnetic films is the double layer films reported by Siegle (4). These films are made of two successively deposited uniaxial film layers with their uniaxial easy axes at right angle to each other. The usual uniaxial anisotropy of these composite films vanishes and is replaced by a field-dependent biaxial anisotropy. This biaxial anisotropy vanishes in the limit of large

orienting fields. Theoretical analysis relates this biaxial property to exchange coupling between the two halves of the double-layer films. In this case, the biaxial anisotropy is proportional to the magnitudes of uniaxial anisotropies of the composite films. The important facts about this type of biaxial films is that the uniaxial anisotropy and thickness of each of the two film layers has to be kept the same. The switching characteristics of this type of composite film has been studied by Goto et al. (8), in which they have extended the analysis to multi-layer films with biaxial and triaxial terms. As a special case, the influence of these multiaxial terms on the form of the critical switching curves are studied both theoretically and experimentally. The experimental results of an ordinary uniaxial film with a deposited thin layer of Ni-Co show a considerable improvement of the pulse coincidence switching characteristics.

The biaxial anisotropy described in this thesis is different from all the above mentioned ones in that it is a result of the shape effect of the entire film element. Although it is field-dependent and vanishes in the limit of infinite orienting field, this does not preclude it from practical device applications. For finite orienting field (12 to 14 Oe) the large measured biaxial anisotropy term of the star-film makes it a potentially useful biaxial memory element.

The star-shaped film as well as large plane of these elements can be easily fabricated by photo-etching techniques. The only difficulty in making a pure biaxial element is the fabrication of an isotropic film. However, in some cases, biaxial element with complex biaxial anisotropy

(biaxial with admixed uniaxial anisotropy) is rather desirable (5) because it is less disturb sensitive in memory operation.

II. MAGNETIZATION DISTRIBUTION IN THIN MAGNETIC FILM OF SYMMETRICAL SHAPE WITH NO ORIENTING FIELD

A. Theoretical Formulation

Maxwell's equations governing the magnetic fields of a magnetic film element as shown in Figure 6 can be expressed as follows:

Internal fields: Region I

$$\underline{B}_1 = \mu_o(\underline{H}_1 + \underline{M})$$

$$\nabla \cdot \underline{B}_1 = 0 \quad \text{which gives} \quad \nabla \cdot \underline{M} = - \nabla \cdot \underline{H}_1$$

$$|\underline{M}(\underline{r})| = M_o = \text{constant}.$$

External fields: Region II

$$\underline{B}_2 = \mu_o \underline{H}_2$$

$$\nabla \cdot \underline{B}_2 = 0$$

$$\nabla \times \underline{H}_2 = 0$$

$$\underline{H}_2(\underline{r}) = 0 \quad \text{as} \quad r \text{ goes to infinity.}$$

Boundary conditions:

$$\underline{H}_1^t = \underline{H}_2^t \; ; \text{ continuity of tangential H-fields,}$$

$$\underline{B}_1^n = \underline{B}_2^n \; ; \text{ continuity of normal B-fields.}$$

Energy relations: (9,10)

$$E_T = E_m + E_a + E_{ex}$$

where

E_T = total energy,

E_m = magnetic energy $= \frac{1}{2} \int \underline{H}_1 \cdot \underline{M} \, dv$

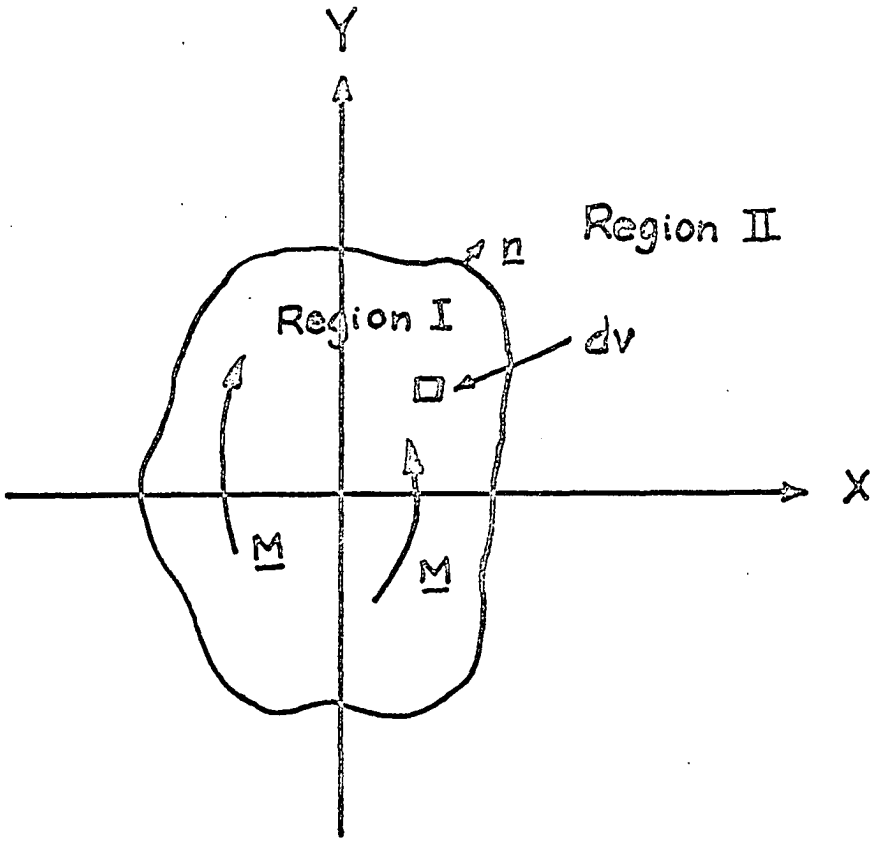

Figure 6. An irregular-shaped magnetic film

E_a = anisotropy energy = $-\frac{1}{2}\int \underline{H}_a \cdot \underline{M}\, dv$

E_{ex} = exchange energy = $\int c(\text{grad } \underline{M})^2\, dv$

$\underline{H}_1$: the internal field resulting from the volumetric and surface magnetic pole distributions namely $-\nabla\cdot\underline{M}$ and $\underline{n}\cdot\underline{M}$.

$\underline{H}_a$: anisotropy field which is a function of the angle between $\underline{M}$ and the easy-axis of the firm.

c : exchange constant. (11)

The equilibrium condition can be obtained by solving the stationary solution of the energy E_T subjected to the constraint that $\underline{M}\cdot\underline{M} = M_o^2 =$ constant.

Using the Lagrange multiplier method (12), the following equations are obtained:

Consider the variation of $\int(E_T - \lambda\, \underline{M}^2)\cdot dv$ for an arbitrary volume dv, the condition for stationary solution is

$$\delta \int (E_T - \lambda\, \underline{M}^2)\, dv = 0,$$

or
$$\delta \int [\tfrac{1}{2}(\underline{H}_1 - \underline{H}_a) \cdot \underline{M} + c(\text{grad } \underline{M})^2 - \lambda\, \underline{M}^2] dv$$

$$= \int \delta\underline{r}\cdot\{\tfrac{1}{2}[-(\text{grad } \underline{H}_1)\cdot\underline{M} - \underline{H}_1\cdot(\text{grad } \underline{M}) - \underline{H}_a\cdot\text{grad } \underline{M} - (\text{grad } \underline{H}_a)\cdot\underline{M}$$

$$+ c\ \text{grad } (\text{grad } \underline{M})^2 - \lambda\ \text{grad } (\underline{M})^2\}\cdot dv = 0,$$

This equation is satisfied for arbitrary dv, if

$$(\text{grad } \underline{H}_1)\ \underline{M} + \underline{H}_1\cdot(\text{grad } \underline{M}) + \underline{H}_a\cdot(\text{grad } \underline{M}) + (\text{grad } \underline{H}_a)\cdot\underline{M}$$

$$- 2c\ \text{grad } (\text{grad } \underline{M})^2 + 2\lambda\ \text{grad } (\underline{M})^2 = 0$$

or in index notation,

$$\frac{\partial (H_1)_i}{\partial x_j} M_j + (H_1)_i \frac{\partial M_i}{\partial x_j} + (H_a)_i \frac{\partial M_i}{\partial x_j} + \frac{\partial (H_a)_i}{\partial x_j} M_i$$

$$- 4 c \frac{\partial M_i}{\partial x_k} \frac{\partial^2 M_i}{\partial x_j \partial x_k} + 4 \lambda M_i \frac{\partial M_i}{\partial x_j} = 0$$

where i, j, k all take the values 1, 2, 3 and repeated indices are summed over.

These are the equations to be solved to give the minimum energy of the film element. To see the above equations are sufficient to solve the problem, the number of unknowns and the number of equations are compared as follows:

Number of unknowns: $\underline{B}_1$, $\underline{H}_1$, $\underline{B}_2$, $\underline{H}_2$ - 12 independent components, $\underline{M}$ - 3 independent components, λ - 1 component - total of 16.

Number of equations:

$\underline{B}_2 = \mu_o \underline{H}_2$ ----------3

$\nabla \cdot \underline{B}_2 = 0$ ----------1

$\nabla \times \underline{H}_2$ ----------3

$\underline{B}_1 = \mu_o (\underline{H}_1 + \underline{M})$ ----------3

$\nabla \cdot \underline{B}_1 = 0$ ----------1

$H_2^t = H_1^t$ ----------3

$B_2^n = B_1^n$ ----------1

There is a total of 15 equations.

The last boundary condition*, $\underline{H}_2(\underline{r}) = 0$ at infinity makes the total required 16 equations.

Thus, theoretically this problem can be solved exactly. However, the difficulties arise from the dependence of $\underline{H}_1$ and $\underline{H}_a$ upon the magnetization vector $\underline{M}$. This makes the above minimization a non-linear variational problem which so far appears to be a hopelessly complicated one. To solve it exactly becomes almost an impossible task (13).

B. Approximation by Discrete Magnetization

Several ways have been used to approximate the demagnetizing fields in non-ellipsoidal bodies (13,14,15). In this approximation, region I of the film is divided into small square partitions. Within each partition the magnetization $\underline{M}_{i,j}$ is assumed to be uniform, so there is no $-\nabla\cdot\underline{M}$. Only on the four sides of the square are there magnetic free poles, i.e., on top and bottom sides, the pole densities are $\pm M_{i,j} \cos \alpha_{i,j}$, and on the right and left, $\pm M_{i,j} \sin \alpha_{i,j}$ respectively, where α_{ij} are the angles between $\underline{M}_{i,j}$ and the easy-axis of the film. On the edge of the whole film element, the surface pole distributions are $\underline{n}\cdot\underline{M}_{i,j}$. The magnetic field at the center of each square is then calculated according to this discrete distribution of poles. The calculated field together with the anisotropy field are substituted into the minimum energy relation to obtain a new equilibrium angle $\alpha_{i.j}$ subjected to the constraint of constant $|\underline{M}|$. This process is repeated until the final equilibrium angle is obtained. The numerical method of calculating $\alpha_{i,j}$ is shown in Appendix A.

---

*Dr. S. Liu, Iowa State University, Ames, Iowa. On the Electromagnetic Fields. Private communication, 1965.

For a magnetic thin film with a geometrical shape that is energetically favorable to stay in a single domain (such as a memory element) this iterative process can be applied to find the magnetization distribution. In this case, the accuracy of the distribution is believed to be dependent on the fineness of the square size. Theoretically speaking, in the limiting case, as the size goes to zero, this process should give a continuous distribution of $\underline{M}$.

With the aid of a digital computer, the calculations can be performed with ease. However, to start this calculation, an initial distribution of $\underline{M}$ has to be assumed. With a known geometry of the film a properly assumed distribution of $\underline{M}$ could give a faster convergence of $\alpha_{i,j}$. With a symmetric film element, the initial $\underline{M}$ can even be assumed to be uniformly distributed along the easy-axis.

C. Choice of Geometric Shape of Film Element

Since an ellipsoid is a stationary state for a magnetized body to have uniform distribution of $\underline{M}$ and uniform demagnetizing field, and also the normalized demagnetizing fields for various ellipsoidal dimensions have been tabulated (16). Also, it has been theoretically proved (1) that an arbitrary single - domain particle in a uniform applied field behaves like a suitably chosen ellipsoid of the same volume, so the geometric shape of a planar film element having the same length and volume as an suitable ellipsoid has been chosen in this investigation.

The result of transforming (see Appendix b) an ellipsoid into a planar film of the same length and volume as shown in Figure 14 is:

$$Y = \frac{\pi bc}{2t}\left(1 - x^2/a^2\right)$$

where a > b >> c, are the axes of the ellipsoid, and t is the thickness of the planar film. Thus, the resulting geomerty of the planar film has the shape enclosed by two parabolas intersected at the points $(\pm a, 0)$ in the X-Y plane.

D. Examples

The demagnetizing fields and the corresponding $\underline{M}$-distributions have been calculated for two film elements of the above described shape (L=2a=2 cm, W=2b=1 cm, T=πbc/2) but with different thicknesses (Film No. 1, T=500 A; Film No. 2; T=20,000A). The size of the square partition is .05 cm x .05 cm x T. The initial $\underline{M}_{i,j}$ are assumed to be pointing in the direction of the easy-axis which is along the line joining the two intersections of the enclosed parabolas.

The first iteration of $\alpha_{i,j}$ gives satisfactory results for Film No. 1 (T=500 A). The calculated demagnetizing fields and $\alpha_{i,j}$ along the film element are shown in Figures 7 and 8.

For Film No. 2 (T=20,000 A), agreeable results of $\alpha_{i,j}$ are obtained for most part of the film element except regions very near the edge and the tips where it is understood to have the highest pole concentrations. Iterations up to 9th time have been calculated. The $\underline{M}$-distributions of the 9th-iteration are shown in Figure 9.

From the results of the first iteration, it is seen that minimum energy condition tends to diffuse the free surface poles into the film. This agrees with observations of $\underline{M}$ which usually follows the physical

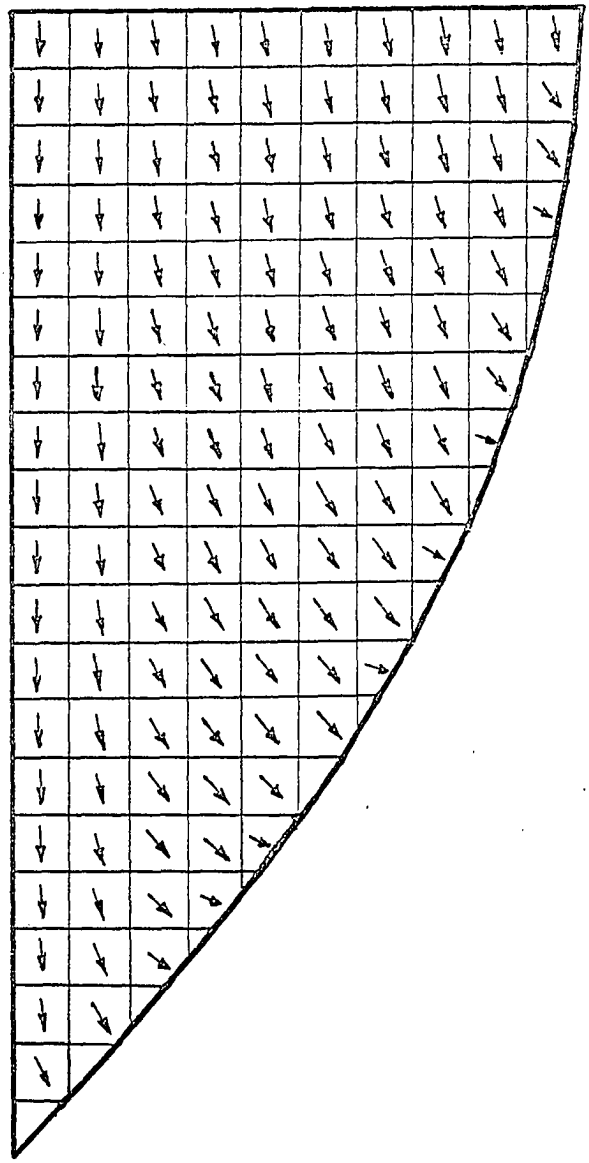

Figure 7. Orientations of demagnetizing fields for the 500 Å film element

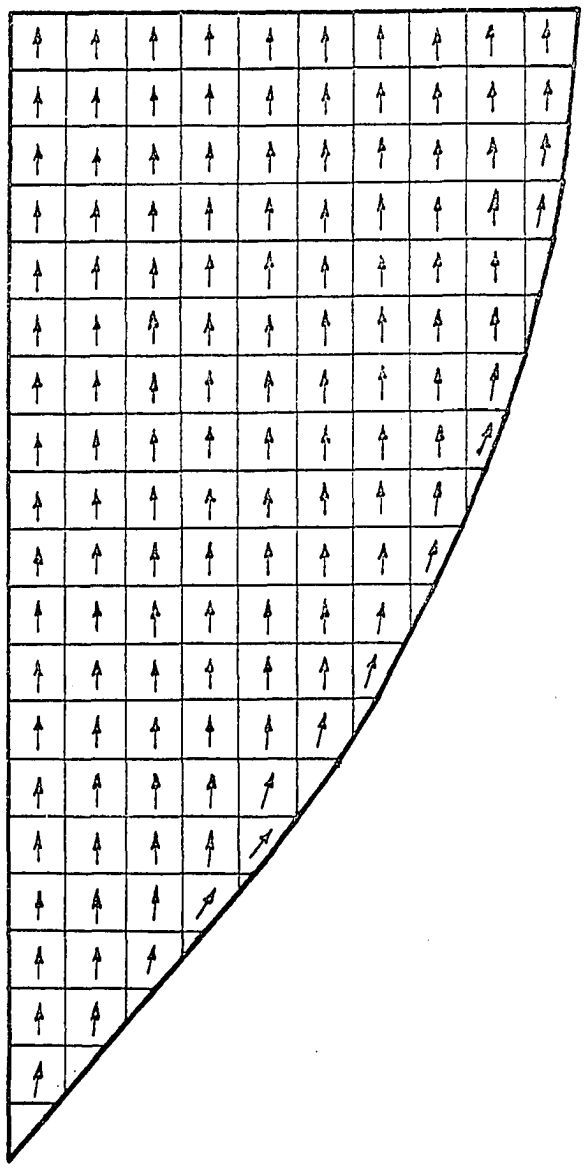

Figure 8. M-distribution for the 500 Å film element

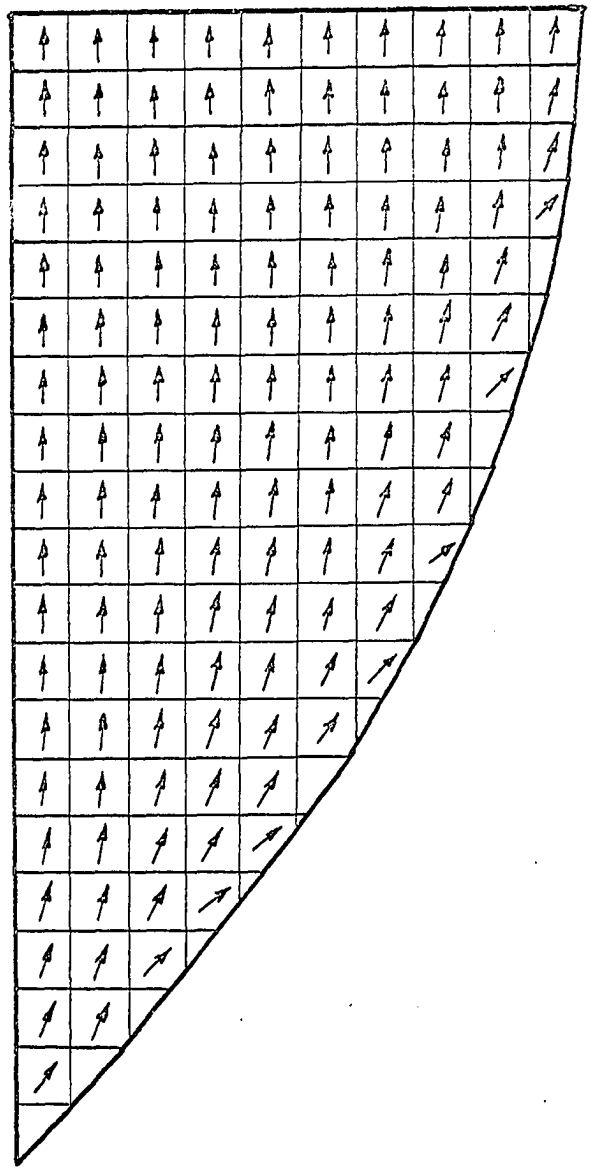

Figure 9. M-distribution for the 20,000 Å film element

boundary of the film element.

To take into account of the edge effect as having been done for Film No. 2, the partitions in the tip regions are further subdivided by one half of their original size. Demagnetizing field at the center of each partition is calculated and energy minimized. After 9 such iterations, $\alpha_{i,j}$'s along the central region begin to repeat themselves. These are the equilibrium angles of the corresponding $\underline{M}_{i,j}$'s under the assumed conditions.

In the course of these calculations, the computer program has been essentially the same except everytime when the partitions are halved, the charge distribution arrays are quadrupled, so is the computing time. It is believed that by further sub-division of the partitions, the region of convergence of $\alpha_{i,j}$ will expand and eventually will cover the whole film element as the subdivision process goes on. The limiting case is when the size of the partition approaches zero which reduces to the continuous case. Of course, in the latter case, the exchange energies have to be accounted. In the above calculations only one subdivision of the partitions in the tip regions has been made, and no further subdivisions or iterations have been attempted. However, this calculation does show that the stationary distributions of $\underline{M}$ can be obtained for a two-dimensional case with arbitrary accuracy provided that sufficient partitions are made.

III. CALCULATION OF MAGNETIC ENERGY AND SHAPE INDUCED BIAXIAL ANISOTROPY

A. Assumptions

Consider two film elements as described in previous section are joined perpendicularly as shown in Figure 1. The basic idea is to obtain the magnetic energy difference for the average magnetizations oriented in the 90° (high energy state) and 45° (low energy state) directions. In order to approximate the magnetic energy as close as possible, discrete distributions of magnetization have been used. These first order quasi-equilibrium discrete distributions are obtained under the minimum energy conditions in the presnece of demagnetizing field and the applied orienting field. As a result of the discrete approximation, the $\underline{M}$-distribution becomes non-uniform inside the film element as shown in Figures 2 and 4. Also, to take account only the shape effect, the film is assumed to be completely isotropic. The calculated biaxial anisotropy is then obtained under the assumption that all the excess energy of the former over that of the latter can be attributed to the biaxial property of the film element.

B. Demagnetizing Field and Discrete Approximation of $\underline{M}$-Distributions

The demagnetizing field (10) within a region R can be expressed as:

$$\underline{H}_d = \int_R \frac{\rho_m \underline{r}}{r^3}\, dv + \int_s \frac{\sigma_s \underline{r}}{r^3}\, ds$$

where $\rho_m = -\nabla \cdot \underline{M}$ is the effective volume pole density, $\sigma_s = \underline{n} \cdot \underline{M}$, an effective surface pole density on the surface S of the region R, and $\underline{n}$ is the outward unit normal from S. To conform with the unit used in laboratory measurement of magnetic field, the units used in the above equation and also from

now on throughout this thesis, all dimensions are in cgs units so that the calculated $\underline{H}_d$'s are in units of Oe.

In the discrete approximation of magnetization, the film element is divided into small square partitions. As described in previous section, magnetic pole densities are distributed along the four sides of the partitions. By assuming uniform magnetization within each of the partitions, then the demagnetizing field at the center of the partition (p,q) can be expressed as:

$$\underline{H}_{p,q} = \sum_{i,j} \int_{\ell} \frac{\underline{M}_{i,j}\, \underline{n}_{\ell}}{(r_{i,j})^3}\, \underline{r}_{i,j}\, t\, d\ell$$

where, $\underline{M}_{i,j}$ = the magnetization in partition (i,j),

$\underline{r}_{i,j}$ = the distances from (p,q) to the magnetic charges,

$\underline{n}_{\ell}$ = unit normal of the integration path ℓ,

$d\ell$ = elemental boundary of the sides of the partitions,

ℓ = integration path along the four sides of each partition. In case of film boundary partitions, this path is not square, one branch of it will be the physical boundary of the film element.

The summation is to sum over all the partitions enclosed by the film element. The numerical formulation of the demagnetizing field $\underline{H}_{p,q}$ is shown in Appendix C, its computer program is shown in Appendix D, and the quasi-equilibrium distributions for the average magnetization in the 90° and 45° positions are shown in Figure 2 and Figure 4, respectively.

C. Demagnetizing Energy and Shape-Induced Biaxial Anisotropy

The total energy for any discrete $\underline{M}$-distributions can be expressed as:

$$E_m = -\sum_i^N (\underline{M}_i \cdot \underline{H}_i)\Delta V_i$$

where, $\underline{M}_i$, $\underline{H}_i$ and ΔV_i are the magnetization, demagnetizing field and the volume of the i^{th} partition, N, the total number of the partitions enclosed by the star-shaped film element.

The difference of energies (denoted by E_d) between the average 90°-distribution and that of the 45°-distribution is thus obtained by the above discrete approximation. The energy difference E_d is

$$\begin{aligned} E_d &= E_{m90} - E_{m45} \\ &= \sum_i^N (\underline{M}_i \cdot \underline{H}_i)_{45} \Delta V_i - \sum_i^N (\underline{M}_i \cdot \underline{H}_i)_{90} \Delta V_i \\ &\simeq \Delta V \sum_i^N [(\underline{M}_i \cdot \underline{H}_i)_{45} - (\underline{M}_i \cdot \underline{H}_i)_{90}] \end{aligned}$$

where 45 and 90 indicate the quantities for the average magnetizations in the 45° and 90° positions respectively. Since the demagnetizing field calculated here is normalized against the ratio of the thickness T to the length L of the sample, the demagnetizing field can be expressed as

$$\underline{H} = \frac{T}{L} \underline{h}_i$$

where $\underline{h}_i$ is the normalized demagnetizing field against the ratio of T/L. The ratio of T/L used in this investigation is 0.0001. Also the magnetization vector can be written as

$$\underline{M}_i = M\underline{a}_i$$

where $\underline{a}_i$ is the unit vector pointing in the direction of $\underline{M}_i$ and M, the magnitude of $\underline{M}_i$. Then E_d can be reduced to

$$E_d \cong \Delta V \frac{MT}{L} \sum_{i}^{N} [(\underline{a}_i \cdot \underline{h}_i)_{45} - (\underline{a}_i \cdot \underline{h}_i)_{90}] .$$

The energy contribution due to biaxial anisotropy in a thin film in the presence of an applied field is:

$$E_{k2} = \frac{V}{4} K_2 \sin^2 2\phi$$

where K_2 = biaxial anisotropy constant,

$V = N \Delta V$ = total volume of the film,

ϕ = angle between $\underline{M}$ and reference easy axis.

Equating the magnitude of this energy to that of the difference energy E_d, the calculated biaxial anisotropy constant K_2 is obtained, i.e.,

$$K_2 = \frac{4E_d}{V} = \frac{4MT}{NL} \sum_{i}^{N} [(\underline{a}_i \cdot \underline{h}_i)_{45} - (\underline{a}_i \cdot \underline{h}_i)_{90}]$$

Note that the biaxial anisotropy constant follows the definition given by Pugh (5), only in this case K_2 is dependent on the geometrical shape of the film element.

The equivalent shape-induced biaxial anisotropy field H_{K_2} can also be defined as:

$$H_{K_2} = 2 K_2/M = \frac{T}{L} \frac{8}{N} \sum_{i}^{N} [(\underline{a}_i \cdot \underline{h}_i)_{45} - (\underline{a}_i \cdot \underline{h}_i)_{90}] .$$

To express the thickness T in units of 1000 Å and the length in mm, we can define a biaxial anisotropy field constant K for the star-shaped film as:

$$K = \frac{0.008}{N} \sum_{i}^{N} [(\underline{a}_i \cdot \underline{h}_i)_{45} - (\underline{a}_i \cdot \underline{h}_i)_{90}] \cdot$$

Note the $\underline{h}_i$'s are dependent on the shape factor L/W which is the ratio of the length to the width of the star film (see Figure 1), so K is also a function of L/W.

In summary, the shape induced biaxial anisotropy field can be expressed in a simple form as:

$$H_{K_2} = K\ T/L$$

where, K = K (L/W) = biaxial anisotropy field constant in Oe, and is a function of L/W,

L = length of film element in mm,

W = width of film element in mm,

T = thickness of film in units of 1000 Å.

For the case of L/W = 10/3, which is used in this investigation, K = 1.12 Oe. Based on the above formula, the film size can be made as small as practical for a desired H_{K_2}.

IV. EXPERIMENTAL RESULTS

A. Theoretical Foundation

The energy equation of a thin magnetic film with mixed uniaxial and biaxial anisotropies under applied field is:

$$E = -MH_x\cos(\phi-\theta) + MH_y\sin(\phi-\theta) + K_1\sin^2(\theta+\psi) + \frac{1}{4}K_2\sin^2 2\theta$$

where θ and ϕ are angles between the easy axis and the magnetization $\underline{M}$ and the applied field $\underline{H}$, and ψ indicates that the biaxial easy axes are not necessarily parallel to the uniaxial easy axis. Using previously defined anisotropy fields, the torque equation can be expressed as:

$$T = \frac{\partial E}{\partial \theta} = -MH_x\sin(\phi-\theta) - MH_y\cos(\phi-\theta) + \frac{1}{2}MH_{K1}\sin 2(\theta+\psi) + \frac{1}{4}MH_{K2}\sin 4\theta.$$

Thus, from the torque curve, the uniaxial and biaxial anisotropies can be determined.

In actual torque measurement, the equilibrium position of magnetization is to be found. This is to achieve a torque balance. From the above torque equation, assuming the applied field is in the y-direction, this is equivalent to

$$T = \frac{\partial E}{\partial \theta} = 0 .$$

By rearranging terms and considering the case, $\psi = 0$, this gives:

$$MH_y\cos(\phi-\theta) = \frac{1}{2}MH_{K1}\sin 2\theta + \frac{1}{4}MH_{K2}\sin 4\theta.$$

This equation represents the balance of torque. The term on the left hand side is the torque due to the externally applied field. The first term on the right hand side is a torque which is a material property, the so-called uniaxial anisotropy. The second term is a torque which, in

this case, is induced by the shape of the star film.

B. Measurement Techniques

There are two most common devices of measuring the above mentioned torque. The one which achieves the torque balance by electromechanical means is called an automatic balancing torque magnetometer (17). The other is an electronic torque magnetometer which was suggested by Dr. T. R. Long of the Bell Telephone Laboratories.

In this investigation, a modified electronic torque magnetometer has been used. A schematic diagram which depicts the various field relations is shown in Figure 10. The operation of this torque balance can be described as follows: a film sample is placed horizontally in the center of a pair of crossed Helmholtz coils. One set of the coils supplies the orienting field H_b in the x-direction, the other gives the restoring field H_r in the y-direction. During the measurement a sufficient orienting field is maintained to insure the film sample staying in a single domain state. An oscillating tickle field (H_t : 1000 cps) which is small in amplitude compared with that of H_b is also applied in the same direction. The measurement starts with one of the easy axes of the sample aligned in the x-direction so there is no output from a figure-8 sense coil. This sense coil which is placed directly underneath the film sample with its axis in the y-direction is designed to pick up any flux changes due to the variations of the magnetization of the sample. When the easy axis of the sample is physically rotated away from the x-direction, as is shown in Figure 10, the new equilibrium position of $\underline{M}$ gives rise to a y-component. This y-component of $\underline{M}$ under the influence of the tickle

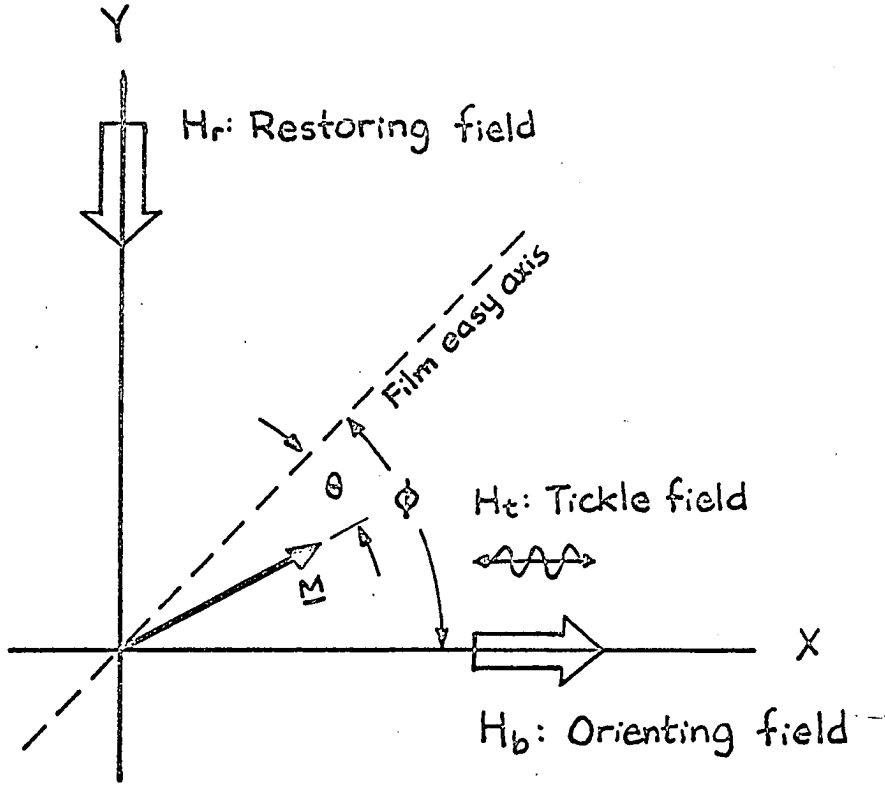

Figure 10. Field relations for the electronic torque magnetometer

field H_t produces an output in the sense coil. The restoring field is then applied, which exerts a torque to restore $\underline{M}$ back to the x-direction, and the amplitude of H_r is adjusted until there is no output from the sense coil. This can be described by the torque equation as:

$$T = \left.\frac{\partial E}{\partial \theta}\right|_{\phi=\theta} = 0$$

or

$$MH_r = \frac{1}{2} MH_{K1} \sin 2\theta + \frac{1}{4} MH_{K2} \sin 4\theta.$$

It is this restoring field which is proportional to the anisotropy torque, and its amplitude versing the sample physical rotation angle gives the torque curve.

C. Preparation of Films

In order to show a pronounced biaxial term in the star-shaped film, the uniaxial anisotropy of the film has to be as small as possible. The anisotropy of a vacuum evaporated film is strongly dependent on the substrate temperature during the deposition (18). The optimum temperature for both low H_{K_1} and ΔH_{K_1} is about 325°C. In the preparation of the film sheets, the substrates were baked around 300 $\sim$ 340°C for at least 45 minutes before the evaporation of Ni-Fe. The H_{K_1}'s of the evaporated films obtained this way were all within a satisfactory range of 2.0 $\sim$ 2.6 Oe. and with thicknesses between 2,000 $\sim$ 6,000 Å.

Arrays of star-shaped elements were photo-etched from these film sheets with the uniaxial axis aligned in the 45° direction as shown in Figure 1. Two different sizes (4mm and 2mm) of the star films were prepared. The larger sized element was then cut from the array and was

measured singly. The smaller ones, due to their low level flux output, were cut in a 3 x 3 array and measured as a gross effect of nine elements.

D. Measured Results

The measured torque curves are shown in Figures 11 and 12. Note the vertical scale is in units of ma which can be easily converted in Oe, in this case, by multiplying a factor of 0.016. These curves are then Fourier analyzed with their Fourier components shown in Table 1. As is shown by the Fourier components of each of these samples, the only significant terms are the second and fourth harmonics which are the contributions of uniaxial and biaxial anisotrophies respectively. All the rest of the terms are of negligible amplitude and are considered to have been introduced by measurement error and instrument drift.

The comparison of the calculated H_{K_2}'s with those of measured are listed in Table 2. An orienting field H_b of 14 Oe has been used for all of the calculated H_{K_2}'s and for those of measured ones several different values of H_b has been used as shown in the table. The accuracy of the calculated H_{K_2}'s is limited by the technique used to measure the thickness of the sample. It is estimated that the measured values of thickness are within $\pm$ 10% of their true values.

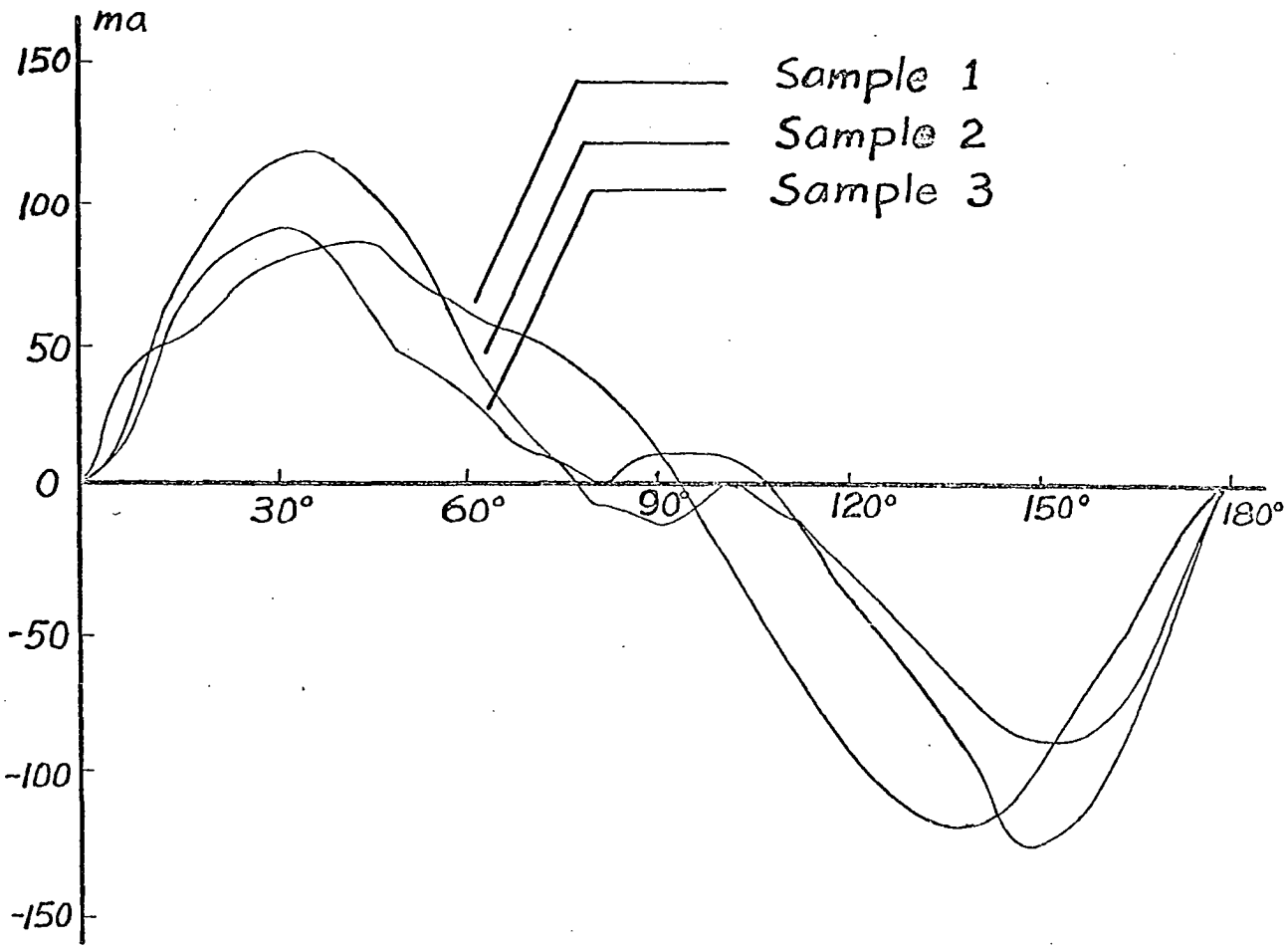

Figure 11. Measured torque curves

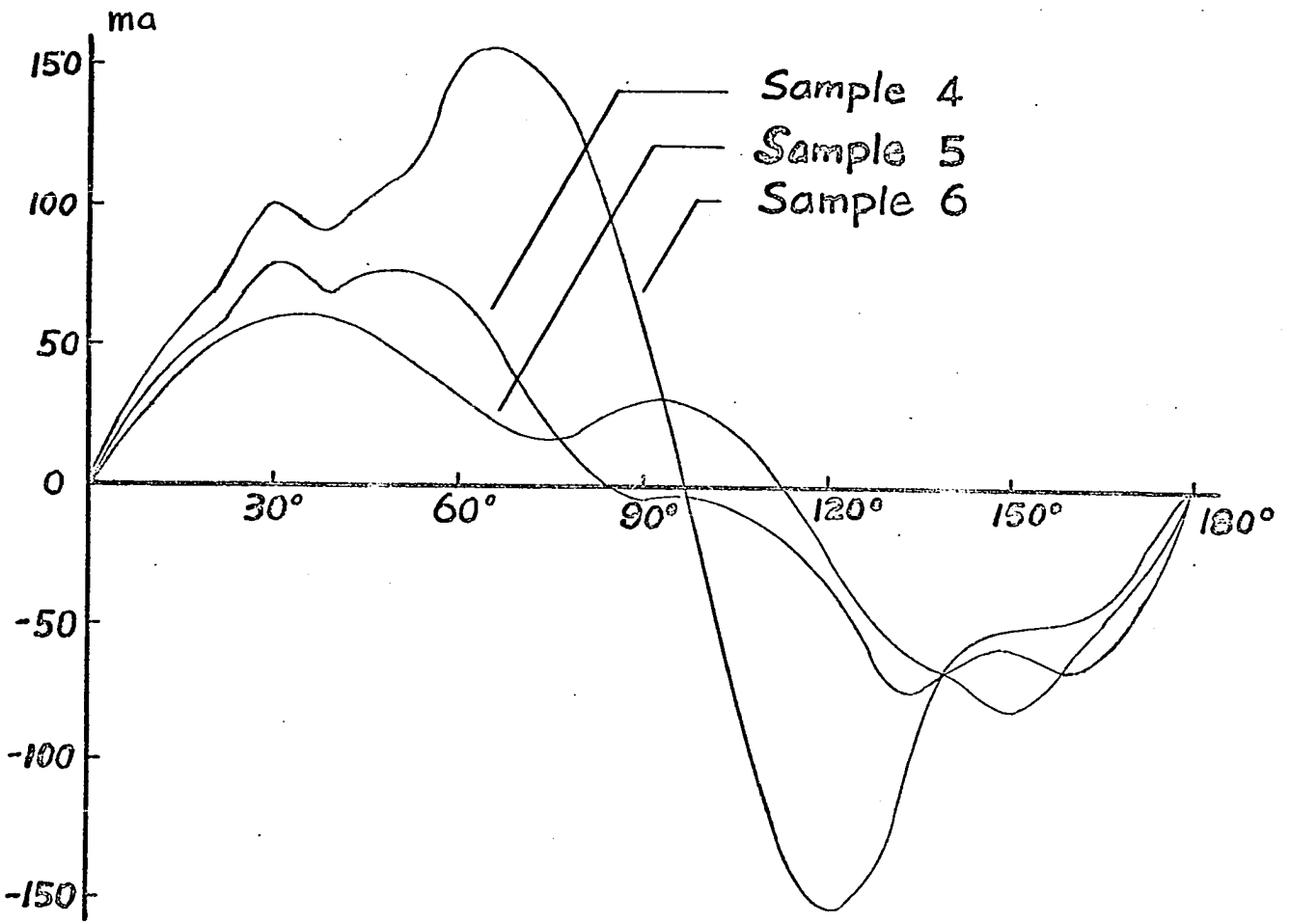

Figure 12. Measured torque curves

Table 1. Fourier components of measured torque curves

Sample	n	0	1	2	3	4	5	6	7	8	9	10
1	cosnθ	-7.5	2.5	1.5	0.1	16.8	-0.2	-3.4	-0.2	1.5	-1.2	0.3
	sinnθ	0.0	0.7	96.1	-1.3	4.0	-1.7	-3.6	-0.1	-0.4	0.3	1.2
2	cosnθ	4.0	-1.3	6.3	1.0	-1.8	-1.3	-1.5	-0.7	-0.6	-0.0	0.3
	sinnθ	0.0	-0.9	77.0	-0.1	31.9	-4.1	-1.4	-2.5	2.1	-2.4	-2.8
3	cosnθ	-4.3	-1.8	-4.5	-0.3	14.8	-1.5	+2.6	-0.4	1.8	-0.8	-2.1
	sinnθ	0.0	-4.1	77.5	-1.9	37.0	-3.8	-1.4	-1.8	0.2	-1.4	-1.8
4	cosnθ	4.0	-0.1	2.6	-0.3	-3.3	0.0	-0.3	-0.0	-1.0	0.3	1.9
	sinnθ	0.0	1.1	67.0	-1.1	17.8	-1.8	-5.7	0.0	6.7	-1.4	-1.6
5	cosnθ	1.3	-1.0	-9.7	0.2	15.1	-0.4	1.1	-0.2	1.4	-0.5	-0.9
	sinnθ	0.0	2.2	58.8	-0.1	24.9	-1.7	-2.5	-1.6	1.5	-1.5	-1.3
6	cosnθ	7.1	-2.4	-107.3	3.5	30.5	-0.3	7.8	-0.6	4.3	-1.3	-4.5
	sinnθ	0.0	1.1	71.2	-1.2	27.1	-3.5	-22.6	0.4	-1.8	-0.2	-3.1

Table 2. Comparison of measured and calculated H_{K_2}'s

Sample	Size (mm^2) L x W	Thickness (Å)	H_b(Oe)	H_{K_1} (Oe)	H_{K_2} (Oe)	
					meas.	calc.*
1	2 x 0.6	1800	6.6	3.08	1.11	1.01
2	2 x 0.6	2900	6.6	2.46	2.08	1.68
3	2 x 0.6	3300	6.6	2.48	2.59	1.75
4	4 x 1.2	3300	12.0	2.14	1.14	0.92
5	4 x 1.2	5700	9.0	2.07	1.88	1.59
6	4 x 1.2	8000	9.0	3.84	2.61	2.23

*The error in the calculated value is estimated to be within $\pm$ 10% which is introduced by the thickness measurement of the sample.

V. DISCUSSION

In this investigation, biaxial anisotropy arising from an appropriately shaped thin magnetic film, has been experimentally measured. A mathematical model based strictly on the shape dependent demagnetizing fields has been derived to estimate this shape induced biaxial term. The shape used in this investigation to induce the biaxial term is a four pointed star. Its biaxial contributions were also measured in a more direct fashion by means of a modified torque magnetometer technique and compared with the above calculated values. The comparisons were in close agreement for samples with various thicknesses and dimensions as listed in Table 2. It is seen from this table that for the star-shaped film under a constant orienting field the measured biaxial anisotropy field H_{K_2} increases as the thickness of the film is increased. Since the demagnetizing field is directly proportional to the thickness of the film, this measured result further substantiates the assumption that the biaxial anisotropy of the star-shaped film is derived from the demagnetizing energy of the film element. Also the measured values of H_{K_2}'s are all higher than those of the corresponding calculated ones as indicated in the table. This is because H_{K_2} is field-dependent and that all of the values of the orienting field used in the measurements are considerably lower than the one (14 Oe) used for all of the calculated ones.

According to Brown's theorem (1) that the magnetic energy for the star film will be independent of the orientation of the magnetization if the latter is assumed to be uniform. For finite orienting field the uniform magnetization can not be established due to demagnetizing field

which varies both in magnitude and direction from point to point inside the film. Instead the magnetization distributes itself in such a way that in presence of the orienting field and the demagnetizing field the total energy of the film is minimized. This minimum energy condition gives a result of non-uniform distribution of magnetization in the star film. To simulate this non-uniform distribution of magnetization, the star film is divided into small square partitions and a discrete distribution of magnetization is assumed. The demagnetizing field at the center of each partition is calculated according to an initial distribution of magnetization and then the equilibrium angle of magnetization vector is calculated under the minimum energy condition in presence of this demagnetizing field and an externally applied orienting field. Each time a new distribution magnetization is obtained and so is a new set of demagnetizing fields. The final quasi-equilibrium non-uniform distribution of magnetization is obtained by iteration process.

The 90° and 45° distributions of magnetization (see Figures 2 and 4) are respectively corresponding to the orienting field applied in the directions of 90° and 45° measured from the film axis as shown in Figure 1. The calculated results show that the 90°-distribution gives the highest energy and the 45°-distribution, the lowest energy. It is the energy difference between these two distributions of magnetization which gives the biaxial anisotropy of the star film. A numerical calculation was worked out to simulate the uniform magnetization case (which was equivalent to an infinite orienting field). The resulting biaxial anisotropy field was 0.05 Oe (zero in the ideal case) as compared with 1.12 Oe for

that of the non-uniform one.

The potential usefulness of this shape-induced biaxial anisotropy lies in the fact that in practice the applied field is always finite in magnitude. The actual distribution of magnetization in the film is therefore always non-uniform. Thus the field dependence of the biaxial anisotropy does not preclude its use for device applications.

The prerequisite of making a pure biaxial element by shape-effect techniques is to start with an isotropic film. The fabrication of a purely isotropic film has been found to be a non-trivial task. In this investigation, the star-shaped elements were etched from uniaxial films. As a result of the inherent uniaxial anisotropy, they all possessed mixed uniaxial and biaxial properties which were shown clearly in the measured torque curves and their Fourier components. However, in memory applications, a complex biaxial (biaxial with admixed uniaxial anisotropy) film is desirable for the reason that it is less likely to be disturb sensitive than a film with pure biaxial anisotropy (5). With the formula derived in Section III, the proportion of this admixture can be closely controlled by appropriately chosen values of H_{K_1}, thickness, and length (i.e. tip to tip dimension) of the star-shaped element.

In the numerical calculation of the equilibrium positions for the discrete $\underline{M}$-distributions, usually the $\underline{M}$'s in the central regions of the film element converge to their final positions within 2 to 3 iterations. The $\underline{M}$'s of the partitions in the tip regions and along most boundary regions always oscillate back and forth. In principle the edge effect probably can be solved by further subdivision of the partitions in these

regions progressively as they approach the edge of the film. This technique would approach the continuous distribution as a limiting ease. However, for an engineering problem with limited budget, the partitions are divided as small as practical and the contributions due to these boundary partitions can be even neglected as it has been done in this investigation.

VI. BIBLIOGRAPHY

1. Brown, W. H., Jr. and Morrish, A. H. Effect of a Cavity on a Single-domain Magnetic Particle. Phys. Rev. 105:1198-1201. 1957.

2. Boyd, E. L. Magnetic Anisotropy in Single-Crystal Thin Films. IBM J. Res. Dev. 4:116-129. 1960.

3. Prosen, R. J., Gondo, Y. and Gran, B. E. Origin of Biaxial Anisotropy in Polycrystalline Films. J. of Appl. Phys. 35:826-827. 1964.

4. Siegle, W. T. Exchange Coupling of Uniaxial Magnetic Thin Films. J. of Appl. Phys. 36:1116-1117. 1965.

5. Pugh, E. W. Magnetic Memory Elements with Biaxial Anisotropy. Intermag. Conf. Proc. 1963:15.1-1-15.1-6.

6. Lo, D. S. and Torok, E. J. Magnetic Switching in Epitaxially Grown Ferromagnetic Films. Intermag. Conf. Proc. 1965:2.1-1-2.1-4.

7. Lo, D. S. Magnetic Switching in Ni-Fe Single-Crystal Films. J. Appl. Phys. 37:3246-3258. 1966.

8. Goto, E., Hayashi, N., Honma, N., Kuroda, R. and Miyashita, T. Switching Characteristics of Composite Magnetic Thin Films. Japanese J. of Appl. Phys. 4:712-720. 1965.

9. Kittel, C. K. Physical Theory of Ferromagnetic Domains. Rev. of Mod. Phys. 21:541-583. 1949.

10. Brown, W. F., Jr. Magnetostatic Principles in Ferromagnetism. Amsterdah, Holland, North-holland Publishing Company. 1962.

11. Kittel, C. K. Introduction to Solid State Physics. 2nd ed. New York, New York, John Wiley and Sons, Inc. 1963.

12. Goldstein, H. Classical Mechanics. Reading, Massachusetts, Addison-Wesley Publishing Company, Inc. 1959.

13. Brown, W. F., Jr. and LaBonte, A. E. Structure and Energy of One-dimensional Domain Wall in Ferromagnetic Thin Films. J. of Appl. Phys. 36:1380-1386. 1965.

14. Joseph, R. J. and Schlomann, E. Demagnetizing Field in Nonellipsoidal Bodies. J. of Appl. Phys. 36:1579-1593. 1965.

15. Kump, H. J. Demagnetization of Flat Uniaxial Thin Film under Hard Direction Drive. IBM J. Rev. Dev. 9:118-123. 1965.

16. Osborn, J. A. Demagnetizing Factors for General Ellipsoid. Phys. Rev. 67:351-357. 1945.

17. Humphrey, F. B. and Johnston, A. R. Sensitive Automatic Torque Balance for Thin Magnetic Films. Rev. Sci. Instr. 34:348. 1963.

18. Oredson, H. N. and Torok, E. J. Inhomogeneity in Magnitude of the Anisotropy Field in Thin Nickel-Iron Films. J. of Appl. Phys. 35:810-811. 1964.

VII. ACKNOWLEDGEMENTS

I wish to express my deepest thanks to Dr. A. V. Pohm for his ideas, encouragement, and valuable guidance throughout this work.

I also wish to thank Mr. C. S. Comstock, Jr. for his helpful discussions and especially for his able assistance in the process of depositing magnetic films used in this investigation.

I also wish to extend my appreciation to personnel of the Cyclone Computer Laboratory for their helpful suggestions in the early stage of the numerical calculations; also to the Computation Center of Iowa State University for providing generously the computer time used in this investigation.

VIII. APPENDIX A

EQUILIBRIUM ANGLES OF DISCRETE MAGNETIZATION

The energy density of a thin film is:

$$E = -\frac{1}{2} MH_d \cos(\theta-\phi) + MH_K \sin^2\theta,$$

where H_d = demagnetizing field,

H_K = uniaxial anisotropy field,

θ = angle between $\underline{H}_K$ and $\underline{M}$,

ϕ = angle between $\underline{H}_d$ and $\underline{H}_K$.

The equilibrium position of the magnetization stays where there is a torque balance, i.e.,

$$\frac{\partial E}{\partial \theta} = \frac{1}{2}[MH_d \sin(\theta-\phi)] + 2\, MH_K \sin\theta\, \cos\theta = 0$$

or

$$(H_d\cos\phi)\sin\theta - (H_d\sin\phi)\cos\theta + 4H_K \sin\theta\, \cos\theta = 0 .$$

Choose x-axis in the direction of $\underline{H}_K$, then the demagnetizing field can be expressed in component forms, i.e.,

$$H_x \sin\theta - H_y \cos\theta + 4H_K \sin\theta\, \cos\theta = 0.$$

A computer program designed to solve this equilibrium angle θ is of an iterative type. The general idea of this program is described as follows: a small increment of angle as a perturbation is applied to the torque balance equation. It is then checked against a predetermined deviation from the equilibrium angle θ. When the absolute value of this increment falls below the desired tolerance, the iterations are terminated.

Mathematically, this is done by letting $\Delta\theta$ be the increment, and

substituting into the torque balance equation, i.e.,

$$H_x \sin(\theta+\Delta\theta) - H_y \cos(\theta+\Delta\theta) + 4H_K \sin(\theta+\Delta\theta)\cos(\theta+\Delta\theta) = 0 \ .$$

For small angle $\Delta\theta$, we have $\sin\Delta\theta \cong \Delta\theta$, $\cos\Delta\theta \cong 1$, and using typical value of H_K (3 Oe), this becomes

$$H_x(\sin\theta + \Delta\theta\cos\theta) - H_y(\cos\theta - \Delta\theta\sin\theta) + 12(\sin\theta + \Delta\theta\cos\theta)(\cos\theta - \Delta\theta\sin\theta) = 0.$$

Solving for $\Delta\theta$, we have

$$\Delta\theta = \frac{H_x\sin\theta - H_y\cos\theta + 12\sin\theta\cos\theta}{(12\sin\theta - H_y)\sin\theta - (12\cos\theta + H_x)\cos\theta} \ .$$

A flow-chart illustrating the computer calculation of θ is shown in Figure 13. It can be interpreted in the following manner:

The iteration starts initially with $\theta = 0$ for every set of input data H_x and H_y, and calculates a $\Delta\theta$. Then the absolute value of $|\Delta\theta|$ is compared with a pre-determined deviation which is, in this case, one millionth of θ ($0.000001 \times \theta$). If $|\Delta\theta|$ is greater than this deviation, it is then added algebraically to the currently running θ and fed back to the calculation loop. This iterative process goes on until the value of $|\Delta\theta|$ is smaller or equal to the deviation. However, to prevent the computer from looping in a time consuming divergent case, a counter (I, in the flow-chart) is included to count the number of iterations. When the number of iterations exceeds the preset number (in this case, it is set at 50), it will branch out of the iteration loop and print out "NO CONVERGENCE", and then proceeds to take the next set of data. When the last set of data is sensed, the calculation is terminated.

This iterative process has found to be very effective. In most of

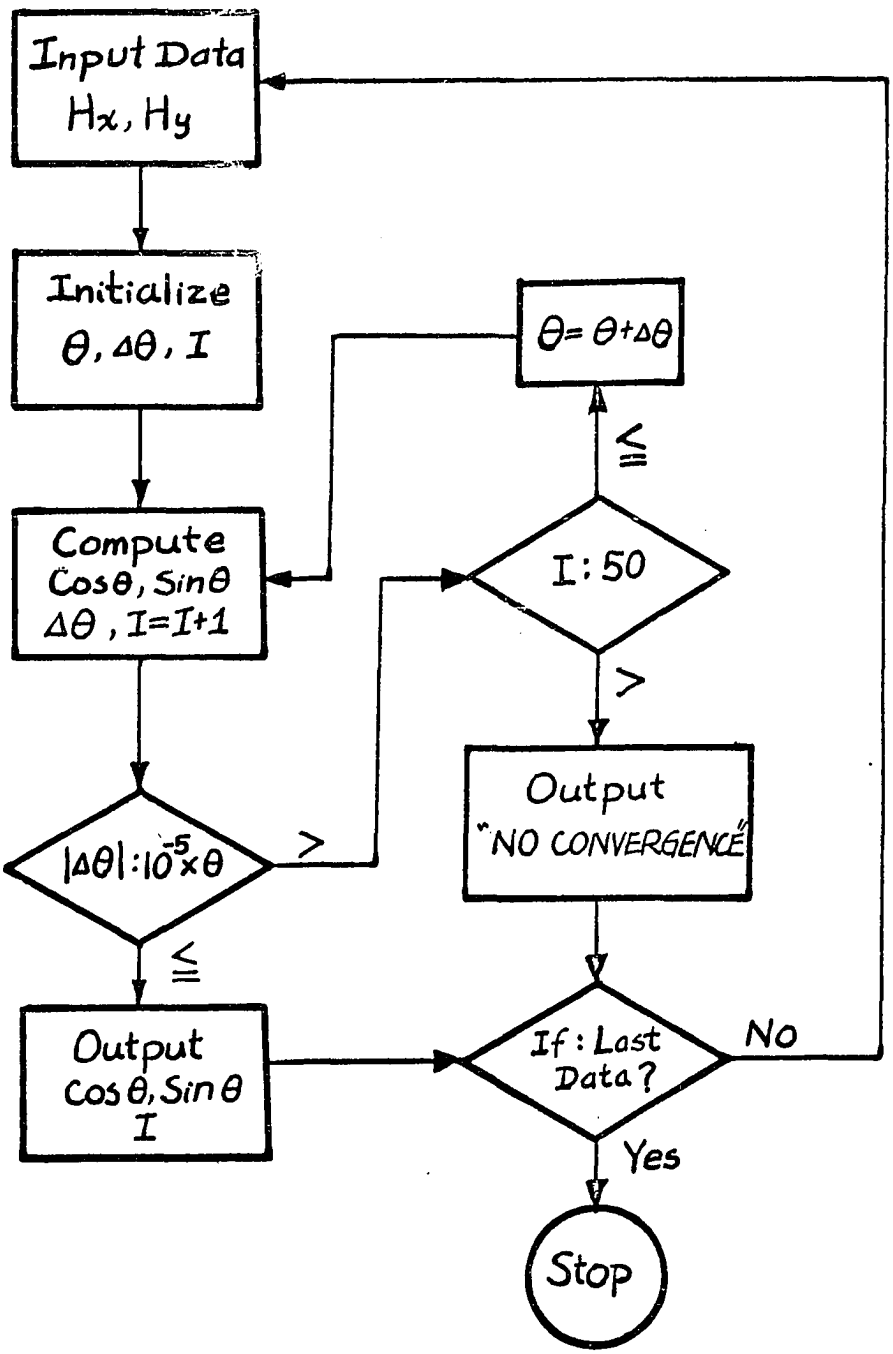

Figure 13. Flow chart for the calculations of equilibrium angles of M-distribution

the cases the convergence of θ takes only 2 to 5 iterations. It also eliminates the tedious and laborious procedures of solving the higher order (4th, in this case) equation algebraically.

IX. APPENDIX B

ELLIPSOIDAL TO PLANAR FILM TRANSFORMATION

This is to transform a 3-dimensional ellipsoid into a planar geometry which has the same length and same volume as those of the ellipsoid (see *Figure 14*). *For the ellipsoid, we have*

$$\frac{x^2}{a^2} + \frac{y^2}{b^2} + \frac{z^2}{c^2} = 1$$

where a > b >> c are the major axes in x and y directions, and minor axis in z direction respectively.

The cross-sectional area perpendicular to the x-axis in y-z plane is an ellipse with the equation

$$\frac{y^2}{b^2} + \frac{z^2}{c^2} = 1 - \frac{x^2}{a^2} \quad .$$

Its major and minor axes are:

$$b(y) = b\sqrt{1 - \frac{x^2}{a^2}} = y$$

$$c(y) = c\sqrt{1 - \frac{x^2}{a^2}} = \frac{cy}{b} \quad ,$$

and its area is:

$$A_e = \pi b(y)c(y) = \frac{cy^2}{b} \quad .$$

Using X-Y coordinates for the corresponding planar film, we have the cross-sectional area perpendicular to the x-axis with thickness t, i.e.,

$$Ap = 2tY$$

Equating Ae = Ap, we have

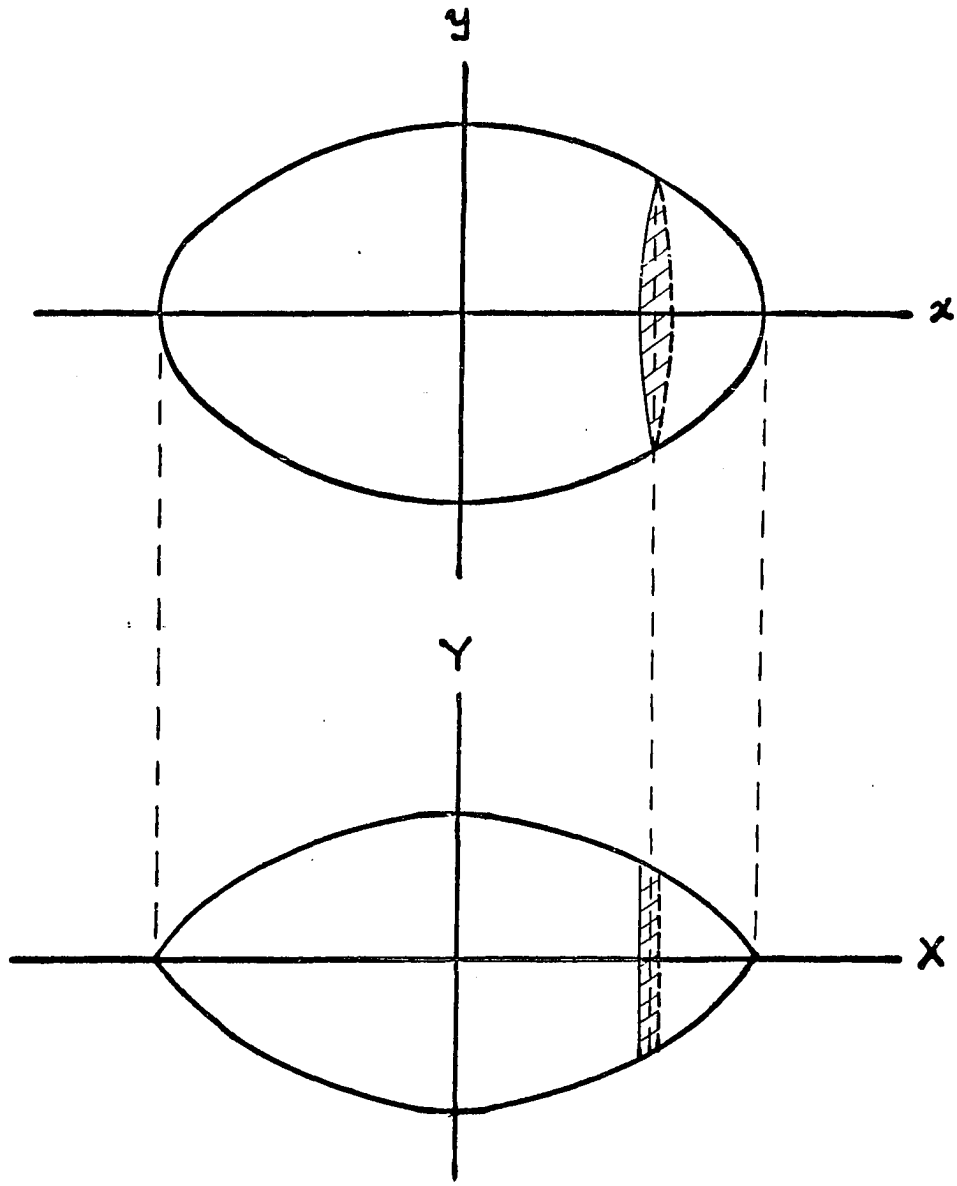

Figure 14. Ellipsoidal to planar film transformation

$$\frac{\pi c}{b} y^2 = 2tY \quad .$$

In the x-y plane, the ellipse is

$$\frac{x^2}{a^2} + \frac{y^2}{b^2} = 1 \quad ,$$

and note that $x = X$, thus the transformed planar geometry in X-Y planes is

$$Y = \frac{\pi bc}{2t} \left(1 - \frac{X^2}{a^2}\right) \quad .$$

X. APPENDIX C

NUMERICAL FORMULATION OF DEMAGNETIZING FIELD IN STAR-SHAPED FILM

The basic formula of calculating the demagnetizing field in a magnetic film of constant thickness is shown in Section III, i.e.,

$$\underline{H}_{p,q} = \sum_{i,j} \int_{\ell} \frac{\underline{M}_{i,j} \cdot \underline{n}_{\ell}}{(r_{i,j})^3} \underline{r}_{i,j} \; t \; d\ell$$

Let the surface charge density be denoted by $\alpha_{i,j} = \underline{M}_{i,j} \cdot \underline{n}_{\ell}$, then the main task of this program is to obtain these various surface charge densities and evaluate the corresponding integrals throughout the film.

When the film is divided into square partitions, there are three different types of surfaces charges, namely, the charges on the vertical and horizontal faces of the interior partitions, and those on the physical boundary of the film.

For the partitions in the interior region of the film, let the magnetization of partition p(i,j) and those of its nearest neighboring partitions p(i+1, j) and p(i, j+1) be expressed in their component forms:

$$\underline{M}_{i,j} = M_o(\underline{i} \cos \alpha_{i,j} + \underline{j} \sin \alpha_{i,j})$$

$$\underline{M}_{i+1,j} = M_o(\underline{i} \cos \alpha_{i+1,j} = \underline{j} \sin \alpha_{i+1,j})$$

$$\underline{M}_{i,j+1} = M_o(\underline{i} \cos \alpha_{i,j+1} + \underline{j} \sin \alpha_{i,j+1})$$

where M_o is the magnitude of $\underline{M}$, $\alpha_{i,j}$, $\alpha_{i+1,j}$ and $\alpha_{i,j+1}$ are the angles of $\underline{M}_{i+1,j}$ and $\underline{M}_{i,j+1}$ respectively, $\underline{i}$ and $\underline{j}$ are the unit vectors in the x and y directions. Note, the convention of indices used here indicates that p(i+1,j) is to the right of p(i,j), and p(i,j+1), on top of p(i,j).

On the vertical interface of p(i,j) and p(i+1,j), with their surface

unit normals $\underline{n}_i = \underline{i}$ and $\underline{n}_{i+1} = -i$, the vertical surface charge density is:

$$C(i,j) = \underline{M}_{i,j} \cdot \underline{n}_i + \underline{M}_{i+1,j} \cdot \underline{n}_{i+1}$$

$$= M_o(\cos \alpha_{i,j} - \cos \alpha_{i+1,j})$$

Call C(i,j) the vertical cosine charge array since it includes all the vertical interface charge densities of all the partitions throughout the interior region of the film.

Similarly, on the horizontal interfaces, a horizontal sine charge array can be expressed as:

$$S(i,j) = M_o(\sin \alpha_{i,j} - \sin \alpha_{i,j+1})$$

The demagnetizing field at point (p,q) due to the cosine array of charges is:

$$\underline{H}_{p,q} = t \sum_{i,j} C(i,j) \int_o^1 \frac{\underline{r}_{i,j}}{(r_{i,j})^3} dy$$

where

$$\underline{r}_{i,j} = (p-i)\underline{i} + (q-j-y)\underline{j} ,$$

$$(r_{i,j})^2 = (p-i)^2 + (q-j-y)^2 ,$$

and for the sine array of charges,

$$\underline{H}_{p,q} = t \sum_{i,j} S(i,j) \int_o^1 \frac{\underline{r}_{i,j}}{(r_{i,j})^3} dx$$

where

$$\underline{r}_{i,j} = (p-i-x)\underline{i} + (q-j)\underline{j}$$

$$(r_{i,j})^2 = (p-i-x)^2 + (q-j)^2 .$$

All these integrals are of the standard forms which are evaluated in most of integrals tables. The summations cover all the interior charge arrays.

Next, calculate the demagnetizing field due to charge distributions on the physical boundary of the star film. This boundary can be divided into eight symmetric branches, and they all have the same general functional form as derived in Appendix B. In the following the demagnetizing field due to the charges on one of the branches in the first quadrant is derived.

Using the above derived function, i.e.,

$$x = \alpha(1 - y^2/a^2)$$

where α is a shape factor determined by the width to length ratio (in this investigation, $\alpha = 1/4$) of the star film, and $a = 1/2$ L, one half of the film length as shown in Figure 1.

Let

$$F(x,y) = x + \frac{\alpha}{a^2} y^2 - \alpha = 0 \ ,$$

then the unit normal out of this boundary surface is:

$$\underline{n} = \frac{\Delta F}{|\Delta F|} = \frac{\underline{i} + \frac{2\alpha}{a^2} y \, \underline{j}}{\sqrt{1 + (\frac{2\alpha}{a^2})^2}}$$

The elemental length along this boundary is:

$$d\ell = \sqrt{1 + (\frac{dx}{dy})^2} \, dy$$

$$= \sqrt{1 + (\frac{2\alpha}{a^2})^2} \, dy \ .$$

So, the elemental charge is:

$$dq_{\ell} = t(\underline{M}_{b,j} \cdot \underline{n})\, d\ell$$

$$= M_o\, t(\cos \alpha_{b,j} + \frac{2\alpha}{a^2}\, y \sin \alpha_{b,j})\, dy$$

where $\alpha_{b,j}$'s are the angles of magnetizations in the partial partitions which form the edge of the film. The demagnetizing field at point (p,q) due to the charges on these edge surfaces is:

$$\underline{H}_{p,q} = \int_b^a \frac{\underline{r}}{(r)^3}\, dq$$

$$= M_o\, t \sum_j \int_o^1 \frac{\underline{r}_{b,j}}{(r_{b,j})^3} (\cos \alpha_{b,j} + \frac{2\alpha}{a^2}\, y \sin \alpha_{b,j})\, dy$$

where

$$\underline{r}_{b,j} = (p-x)\underline{i} + (q-j-y)\underline{j}$$

$$= [p - \alpha(1-y^2/a^2)]\underline{i} + (q-j-y)\underline{j}\ .$$

The summation is used because of discrete approximation of $\underline{M}$.

The contributions to the field due to the rest of the branches are essentially of the same form, provided that appropriate substitutions of coordinates are made in calculating the various unit normals and the distances to the charges, $\underline{r}_{b,j}$'s.

The above integrals can be evaluated by a numerical integration technique called the Simpson's Rules (which is usually a built-in sub-routine in the compilers of most computer systems), or by piecewise linearization of the film boundary. Also, special treatment is required for these non-square boundary partitions to insure conservation of charges. In each of these partitions with one of its four sides forming the physical

boundary of the film, the others are then of non-integral lengths unlike those of a regular interior partition. In the numerical calculation of demagnetizing fields, these irregular lengths are stored in an array, and their contributions are calculated in a separate loop.

The locations of the field point (p,q) inside the film can be obtained in several ways, namely, (a) by direct calculation of maximum q for each increment of p according to the functional relations of the boundary curve, (b) by storing (p,q) in a two dimensional position array, and (c) by storing q in a one dimensional array as a function of increment in p, or vice versa. The last method is found to be the most convenient and time-saving one for the calculations used in this investigation.

The construction of the computer program to solve the demagnetizing fields in the star-shaped film can be described by the simplified flow-chart as shown in Figure 15. The symbols used are as follows:

L: maximum number of partitions,

M: point of intersection,

BL(J) : array of irregular lengths of non-square boundary partitions,

BC(J) : cosine angles of $\underline{M}_{b,j}$ in the boundary partitions (b,j),

BS(J) : sine angles of $\underline{M}_{b,j}$ in the boundary partitions (b,j),

C(I,J) : cosine array of charges of interior partitions,

S(I,J) : sine array of charges of interior partitions,

N(I) : array of field points (p,q),

X1 : the x-component of fields due to BL(J),

Y1 : the y-component of fields due to BL(J),

X2 : the x-component of fields due to C(I,J),

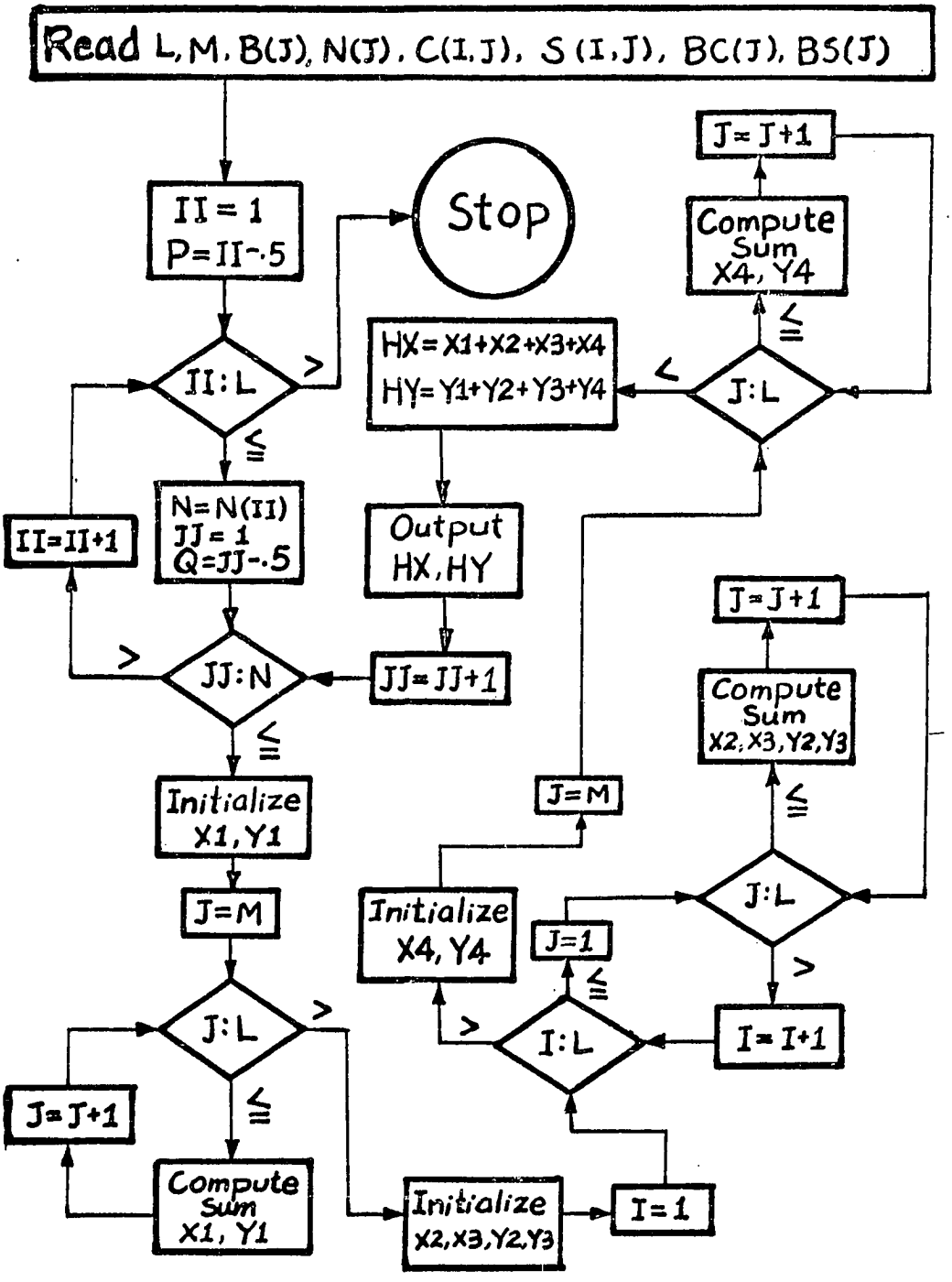

Figure 15. Flow-chart for calculations of demagnetizing fields for the star-shaped film element

Y2 : the y-component of fields due to C(I,J),

X3 : the x-component of fields due to S(I,J),

Y3 : the y-component of fields due to S(I,J),

X4 : the x-component of fields due to curved boundary,

Y4 : the y-component of fields due to curved boundary,

HX : the x-component of total field at (p,q),

HY : the y-component of total field at (p,q).

XI. APPENDIX D

COMPUTER PROGRAM FOR DEMAGNETIZING FIELDS IN STAR-SHAPED FILM

This computer program is in FORTRAN IV language.

```
/JOB                    I0303 FRED LEE  4 MIN
      DIMENSION U1(20),U2(20),F(20),T(20),
     1S2(21,21),QHI(20),QHJ(20),AI(20),BI(20),
     1S1(20,20),CI(20),DI(20)CC1(20),CC2(20)
      REAL MM,K1
      INTEGER U1,U2
      BN(B,C,D,E)=((0.1*C+B)*E-B*D)/(D*E)
      CN(A,B,D,E)=2.*(E-(0.025*B+A)/D)
      FUN(A,B,C)=2./(4.*C*A-B*B)
      ABB(A,B,C)=SQRT(A+0.05*B+0.0025*C)
      READ (1,5) (U1(I),I=1,20)
      READ (1,5) (U2(I),I=1,19)
5     FORMAT (20I3)
      READ (1,6) (F(I),T(I),I=6,20)
6     FORMAT (2F12.7)
      READ (1,77) APF
77    FORMAT (F5.1)
      READ (1,2) L,M
2     FORMAT (2I3)
      MM=-M*0.05
      Y1=-0.25+0.25*MM*MM
      Y3=Y1-0.05
      YMM=4.*MM
      Y411=4.*Y1
      Y433=4.*Y3
      READ (1,99) AXX,AYY,BXX,BYY,CXX,CYY
99    FORMAT (6F12.7)
      AXY=AXX+AYY
      BXY=BXX+BYY
      CXY=CXX+CYY
      DXY=AXY
      EXY=BXY
      FXY=CXY
      WRITE (3,3) L
3     FORMAT (@0   NO. OF ITERATION =@,I3)
      DO 8 I=1,18
      N=U1(I)
      READ (1,7) (CC1(I,J),J=1,N)
7     FORMAT (8F10.7)
8     CONTINUE
      DO 9 J=1,18
      N=U1(J)
      READ (1,7) (S1(I,J),I=1,N)
9     CONTINUE
      READ (1,6) (QHI(I),QHJ(I),I=6,20)
      READ (1,6) (AI(K),BI(K),K=M,19)
      READ (1,6)  (CI(K),DI(K),K=M,19)
      DO 500 II=1,19
      P=-0.5+II
      P11=0.05*P
      KV=U2(II)
```

```
      DO 500 JJ=1,KV
      Q=-0.5+JJ
      Q11=0.05*Q
      QQ=Q11*Q11
C     HORIZONTAL BOUNDARY ELEMENTS
      SHX=0.
      SHY=0.
      DO 100 J=6,20
      QI1=QHI(J)
      QJ1=QHJ(J)
      TJ=T(J)*0.05
      FJ=F(J)*0.05
      Q1=0.05*(Q-J+1)
      Q2=Q1*Q1
      Q3=(Q+J-1)*0.05
      Q4=Q3*Q3
      P1=(P-J+1)*0.05
      P2=P1*P1
      P3=(P+J-1)*0.05
      P4=P3*P3
      QD1=1.0/Q1
      QD3=1.0/Q3
      PD1=1.0/P1
      PD3=1.0/P3
      QF1=Q11-FJ
      QT1=Q11-TJ
      QM1=Q11+TJ
      QM3=Q11+FJ
      PF1=P11-FJ
      PT1=P11-TJ
      PM1=P11+TJ
      PM3=P11+FJ
      PF2=PF1*PF1
      PT2=PT1*PT1
      PM2=PM1*PM1
      PM4=PM3*PM3
      QM2=QM1*QM1
      QM4=QM3*QM3
      QT2=QT1*QT1
      QF2=QF1*QF1
      DFP1=1./SQRT(Q2+PF2)
      DTP1=1./SQRT(Q2+PT2)
      DTM1=1./SQRT(Q2+PM2)
      DTM2=1./SQRT(Q4+PM2)
      DFM1=1./SQRT(Q2+PM4)
      DFM2=1./SQRT(Q4+PM4)
      DPF1=1./SQRT(P2+QF2)
      DPF2=1./SQRT(P4+QF2)
      DPT1=1./SQRT(P2+QT2)
      DPT2=1./SQRT(P4+QT2)
      DMT1=1./SQRT(P4+QM2)
```

```
      DMT2=1./SQRT(P2+QM2)
      DMF1=1./SQRT(P4+QM4)
      DMF2=1./SQRT(P2+QM4)
      DFT2=1./SQRT(Q4+PT2)
      DFP2=1./SQRT(Q4+PF2)
      HHX1=DFP1-DTP1
      HHX2=DTM1-DFM1
      HHX3=DTM2-DFM2
      HHX4=DFP2-DFT2
      HHX5=((Q11-TJ)*DPT1-(Q11-FJ)*DPF1)*PD1
      HHX6=((Q11-TJ)*DPT2-(Q11-FJ)*DPF2)*PD3
      HHX7=((Q11+FJ)*DMF1-(Q11+TJ)*DMT1)*PD3
      HHX8=((Q11+FJ)*DMF2-(Q11+TJ)*DMT2)*PD1
      HHY1=((P11-TJ)*DTP1-(P11-FJ)*DFP1)*QD1
      HHY2=((P11+FJ)*DFM1-(P11+TJ)*DTM1)*QD1
      HHY3=((P11+FJ)*DFM2-(P11+TJ)*DTM2)*QD3
      HHY4=((P11-TJ)*DFT2-(P11-FJ)*DFP2)*QD3
      HHY5=DPF1-DPT1
      HHY6=DPF2-DPT2
      HHY7=DMF1-DMT1
      HHY8=DMT2-DMF2
      H1X=QI1*(HHX1-HHX3+HHX2-HHX4)
      H2X=QJ1*(HHX5-HHX7+HHX6-HHX8)
      H1Y=QI1*(HY15-HY37+HY26-HY48)
      H2Y=QJ1*(HY15-HY37+HY26-HY48)
      SHX=SHX+H1X+H2X
      SHY=SHY+H1Y+H2Y
100   CONTINUE
C     FIELDS DUE TO CORNER ELEMENTS
      PP1=P11+MM+Y1
      PP3=P11-MM-Y1
      PP2=PP1*PP1
      PP4=PP3*PP3
      A1=PP2+QQ
      A2=PP4+QQ
      B1=2.*(PP1-Q11)
      B2=-2.*(PP3+Q11)
      B3=2.*(PP3-Q11)
      B4=-2.*(PP1+Q11)
      CD1=1./(8.*A1-B1*B1)
      CD2=1./(8.*A2-B2*B2)
      CD3=1./(8.*A2-B3*B3)
      CD4=1./(8.*A1-B4*B4)
      T1=2.*A1
      T2=2.*A2
      AP1=PP1+.25
      AP2=AP1*AP1
      AP3=PP1-MM
      AP4=AP3*AP3
      AP5=PP1+Y1
      AP6=AP5*AP5
```

```
AP7=PP1-Y1
AP8=AP7*AP7
AP9=PP1-Y3
P10=AP9*AP9
P15=PP3+Y1
P16=P15*P15
P17=PP3+Y3
P18=P17*P17
P19=PP3-0.25
P20=P19*P19
P21=PP1-0.25
P22=P21*P21
P23=PP3+MM
P24=P23*P23
P25=PP3-Y3
P26=P25*P25
AQ1=Q11-0.25
AQ2=AQ1*AQ1
AQ3=Q11+MM
AQ4=AQ3*AQ3
AQ5=Q11-Y1
AQ6=AQ5*AQ5
AQ7=Q11+Y1
AQ8=AQ7*AQ7
AQ9=Q11+Y3
Q10=AQ9*AQ9
Q13=Q11-Y3
Q14=Q13*Q13
Q19=Q11+0.25
Q20=Q19*Q19
Q23=Q11-MM
Q24=Q23*Q23
SQ11=1./SQRT(AP2+AQ2)
SQ12=1./SQRT(AP8+AQ8)
SQ13=1./SQRT(P10+Q10)
SQ14=1./SQRT(AP4+AQ4)
SQ21=1./SQRT(P18+Q14)
SQ22=1./SQRT(P24+Q24)
SQ23=1./SQRT(P20+Q20)
SQ24=1./SQRT(P16+AQ6)
SQ31=1./SQRT(P20+AQ2)
SQ32=1./SQRT(P16+AQ8)
SQ33=1./SQRT(P24+AQ4)
SQ34=1./SQRT(P18+Q10)
SQ41=1./SQRT(P10+Q14)
SQ42=1./SQRT(AP4+Q24)
SQ43=1./SQRT(AP8+AQ6)
SQ44=1./SQRT(AP2+Q20)
CA11=B1+1.
CA12=B1-Y411
CA13=B1-Y433
```

```
CA14=B1-YMM
CA21=B3+Y433
CA22=B3+YMM
CA23=B3-1.
CA24=B3+Y411
CA31=T1+B1*.25
CA32=T1-B1*Y1
CA33=T1-B1*Y3
CA34=T1-B1*MM
CA41=T2+B3*Y3
CA42=T2+B3*MM
CA43=T2-B3*.25
CA44=T2+B3*Y1
CA51=B2+1.
CA52=B2-Y411
CA53=B2-YMM
CA54=B2-Y433
CA61=B4+Y433
CA62=B4+YMM
CA63=B4+Y411
CA64=B4-1.
CA71=T2+B2*.25
CA72=T2-B2*Y1
CA73=T2-B2*MM
CA74=T2-B2*Y3
CA81=T1+B4*Y3
CA82=T1+B4*MM
CA83=T1+B4*Y1
CA84=T1-B4*.25
CY11=CA11*SQ11-CA12*SQ12
CY13=CA13*SQ13-CA11*SQ11
CY15=CA14*SQ14-CA13*SQ13
CY31=CA21*SQ21-CA22*SQ22
CY33=CA23*SQ23-CA21*SQ21
CY35=CA24*SQ24-CA23*SQ23
CY12=CA31*SQ11-CA32*SQ12
CY14=CA33*SQ13-CA31*SQ11
CY16=CA34*SQ14-CA33*SQ13
CY32=CA41*SQ21-CA42*SQ22
CY34=CA43*SQ23-CA41*SQ21
CY36=CA44*SQ24-CA43*SQ23
CY21=CA51*SQ31-CA52*SQ32
CY23=CA54*SQ34-CA51*SQ31
CY25=CA53*SQ33-CA54*SQ34
CY22=CA71*SQ31-CA72*SQ32
CY24=CA74*SQ34-CA71*SQ31
CY26=CA73*SQ33-CA74*SQ34
CY41=CA61*SQ41-CA62*SQ42
CY43=CA64*SQ44-CA61*SQ41
CY45=CA63*SQ43-CA64*SQ44
CY42=CA81*SQ41-CA82*SQ42
```

```
      CY44=CA84*SQ44-CA81*SQ41
      CY46=CA83*SQ43-CA84*SQ44
      IF (BXY) 20,21,20
20    X12=BXY*(PP1*CY13-CY14)
      X22=EXY*(PP3*CY23+CY24)
      X32=-BXY*(PP3*CY33-CY34)
      X42=-EXY*(PP1*CY43+CY44)
      Y12=BXY*(Q11*CY13+CY14)
      Y22=EXY*(Q11*CY23+CY24)
      Y32=-BXY*(Q11*CY33+CY34)
      Y42=-EXY*(Q11*CY43+CY44)
21    X11=AXY*(PP1*CY11-CY12)
      X13=CXY*(PP1*CY15-CY16)
      X21=DXY*(PP3*CY21+CY22)
      X23=FXY*(PP3*CY25+CY26)
      X31=-CXY*(PP3*CY31-CY32)
      X33=-AXY*(PP3*CY35-CY36)
      X41=-FXY*(PP1*CY41+CY42)
      X43=-DXY*(PP1*CY45+CY46)
      Y11=AXY*(Q11*CY11+CY12)
      Y13=CXY*(Q11*CY15+CY16)
      Y21=DXY*(Q11*CY21+CY12)
      Y23=FXY*(Q11*CY25+CY16)
      Y31=-CXY*(Q11*CY31+CY32)
      Y33=-AXY*(Q11*CY35+CY36)
      Y41=-FXY*(Q11*CY41+CY42)
      Y43=-DXY*(Q11*CY45+CY46)
      X1=(X11+X12+X13)*CD1
      X2=(X21+X22+X23)*CD2
      X3=(X31+X32+X33)*CD3
      X4=(X41+X42+X43)*CD4
      YY1=(Y11+Y12+Y13)*CD1
      YY2=(Y21+Y22+Y23)*CD2
      YY3=(Y31+Y32+Y33)*CD3
      YY4=(Y41+Y42+Y43)*CD4
      HBX=2.*(X1+X2+X3+X4)
      HBY=(YY1+YY2+YY3+YY4)*2.
C     FIELDS DUE TO BOUNDARY
      SUM1=0.
      SUM2=0.
      DO 200 K=M,19
      K1=0.05*K
      F0=0.25-0.25*K1*K1
      01=0.025*K+0.0125
      02=01*01
      P1=P11-F0
      P2=P1*P1
      P3=P11+F0
      P4=P3*P3
      P5=P11-K1
      P6=P5*P5
```

```
P7=P11+K1
P8=P7*P7
Q1=Q11-K1
Q2=Q1*Q1
Q3=Q11+K1
Q4=Q3*Q3
Q5=Q11-F0
Q6=Q5*Q5
Q7=Q11+F0
Q8=Q7*Q7
A1=P2+Q2
A2=P4+Q2
A3=P4+Q4
A4=P2+Q4
A5=P6+Q6
A6=P8+Q6
A7=P8+Q8
A8=P6+Q8
B1=2.*(01*P1-Q1)
B2=-2.*(01*P3+Q1)
B3=-2.*(01*P3-Q3)
B4=2.*(01*P1+Q3)
B5=2.*(01*Q5-P5)
B6=2.*(01*Q5+P7)
B7=2.*(P7-Q7*01)
B8=-2.*(P5+Q7*01)
C1=02+1.
F1=FUN(A1,B1,C1)
F2=FUN(A2,B2,C1)
F3=FUN(A3,B3,C1)
F4=FUN(A4,B4,C1)
F5=FUN(A5,B5,C1)
F6=FUN(A6,B6,C1)
F7=FUN(A7,B7,C1)
F8=FUN(A8,B8,C1)
AB1=ABB(A1,B1,C1)
AB2=ABB(A2,B2,C1)
AB3=ABB(A3,B3,C1)
AB4=ABB(A4,B4,C1)
AB5=ABB(A5,B5,C1)
AB6=ABB(A6,B6,C1)
AB7=ABB(A7,B7,C1)
AB8=ABB(A8,B8,C1)
AA1=SQRT(A1)
AA2=SQRT(A2)
AA3=SQRT(A3)
AA4=SQRT(A4)
AA5=SQRT(A5)
AA6=SQRT(A6)
AA7=SQRT(A7)
AA8=SQRT(A8)
```

```
      BN1=BN(B1,C1,AB1,AA1)
      BN2=BN(B2,C1,AB2,AA2)
      BN3=BN(B3,C1,AB3,AA3)
      BN4=BN(B4,C1,AB4,AA4)
      BN5=BN(B5,C1,AB5,AA5)
      BN6=BN(B6,C1,AB6,AA6)
      BN7=BN(B7,C1,AB7,AA7)
      BN8=BN(B8,C1,AB8,AA8)
      CN1=CN(A1,B1,AB1,AA1)
      CN2=CN(A2,B2,AB2,AA2)
      CN3=CN(A3,B3,AB3,AA3)
      CN4=CN(A4,B4,AB4,AA4)
      CN5=CN(A5,B5,AB5,AA5)
      CN6=CN(A6,B6,AB6,AA6)
      CN7=CN(A7,B7,AB7,AA7)
      CN8=CN(A8,B8,AB8,AA8)
      H1X=(P1*BN1+CN1*O1)*F1
      H2X=(P3*BN2-CN2*O1)*F2
      H3X=(P3*BN3-CN3*O1)*F3
      H4X=(P1*BN4+CN4*O1)*F4
      H5X=(P5*BN5-CN5)*F5
      H6X=(P7*BN6+CN6)*F6
      H7X=(P7*BN7+CN7)*F7
      H8X=(P5*BN8-CN8)*F8
      H1Y=(Q1*BN1-CN1)*F1
      H2Y=(Q1*BN2-CN2)*F2
      H3Y=(Q3*BN3+CN3)*F3
      H4Y=(Q3*BN4+CN4)*F4
      H5Y=(Q5*BN5+CN5*O1)*F5
      H6Y=(Q5*BN6+CN6*O1)*F6
      H7Y=(Q7*BN7-CN7*O1)*F7
      H8Y=(Q7*BN8-CN8*O1)*F8
      QI=AI(K)+BI(K)*O1
      QA=CI(K)*O1+DI(K)
      H13X=H1X-H3X
      H24X=H2X-H4X
      H57X=H5X-H7X
      H68X=H6X-H8X
      H13Y=H1Y-H3Y
      H24Y=H2Y-H4Y
      H57Y=H5Y-H7Y
      H68Y=H6Y-H8Y
      SUM1=SUM1+QI*(H13X+H24X)+QA*(H57X+H68X)
      SUM2=SUM2+QI*(H13Y+H24Y)+QA*(H57Y+H68Y)
200   CONTINUE
C     FIELDS DUE TO COS + SIN ARRAYS OF CHARGES
      HCX=0.
      HCY=0.
      HSX=0.
      HSY=0.
      DO 300 I=1,20
```

```
      KU1=U1(I)
      PII=0.05*I
      PI1=PII-0.05
      P1=P11-PI1
      P2=P1*P1
      P3=P11+PI1
      P4=P3*P3
      P5=P11-PII
      P6=P5*P5
      P7=P11+PII
      P8=P7*P7
      PD1=1.0/P1
      PD3=1.0/P3
      DO 300 J=1,KU1
      SI1=-S1(J,I)
      CI1=-CC1(I,J)
      HSX=HSX+(SX1-SX3+SX2-SX4)*SI1
      HSY=HSY+(SY1-SY3+SY2-SY4)*SI1
      QJJ=0.05*J
      QJ1=QJJ-0.05
      Q1=Q11-QJ1
      Q2=Q1*Q1
      Q3=Q11+QJ1
      Q4=Q3*Q3
      IF (CI1) 210,211,210
C     THE FOLLOWINGS ARE FOR  COS ARRAY OF CHARGES
210   Q5=Q11-QJJ
      Q6=Q5*Q5
      Q7=Q11+QJJ
      Q8=Q7*Q7
      DQJ1=1./SQRT(P2+Q2)
      DQJ2=1./SQRT(P2+Q6)
      DQJ3=1./SQRT(P4+Q2)
      DQJ4=1./SQRT(P4+Q6)
      DMJ1=1./SQRT(P4+Q8)
      DMJ2=1./SQRT(P4+Q4)
      DMJ3=1./SQRT(P2+Q8)
      DMJ4=1./SQRT(P2+Q4)
      CX1=(Q1*DQJ1-Q5*DQJ2)*PD1
      CX2=(Q1*DQJ3-Q5*DQJ4)*PD3
      CX3=(Q7*DMJ1-Q3*DMJ2)*PD3
      CX4=(Q7*DMJ3-Q3*DMJ4)*PD1
      CY1=DQJ2-DQJ1
      CY2=DQJ4-DQJ3
      CY3=DMJ2-DMJ1
      CY4=DMJ4-DMJ3
      HCX=HCX+(CX1-CX3+CX2-CX4)*CI1
      HCY=HCY+(CY1-CY3+CY2-CY4)*CI1
C     THE FOLLOWINGS ARE FOR SINE ARRAY OF CHARGES
211   IF (SI1) 212,300,212
212   DQI1=1./SQRT(Q2+P6)
```

```
      DQI2=1./SQRT(Q2+P2)
      DQI3=1./SQRT(Q4+P6)
      DQI4=1./SQRT(Q4+P2)
      DMI1=1./SQRT(Q2+P4)
      DMI2=1./SQRT(Q2+P8)
      DMI3=1./SQRT(Q4+P4)
      DMI4=1./SQRT(Q4+P8)
      QD1=1.0/Q1
      QD3=1.0/Q3
      SX1=DQI1-DQI2
      SX2=DMI1-DMI2
      SX3=DMI3-DMI4
      SX4=DQI3-DQI4
      SY1=(P1*DQI2-P5*DQI1)*QD1
      SY2=(P7*DMI2-P3*DMI1)*QD1
      SY3=(P7*DMI4-P3*DMI3)*QD3
      SY4=(P1*DQI4-P5*DQI3)*QD3
300   CONTINUE
      HTX=(SHX+HBX+SUM1+HCX+HSX)*0.16
      HTY=(SHY+HBY+SUM2+HCY+HSY)*0.16
      AB=HTX
      BC=HTY-APF
      AC=SQRT(AB*AB+BC*BC)
      ACCC=AB/AC
      ASSS=BC/AC
      AGL=ATAN(BC/AB)*57.2958+180.
      WRITE (2,400) P,Q,HTX,HTY
      WRITE (2,400) P,Q,ACCC,ASSS
400   FORMAT (2F5.1,2F12.7)
      WRITE (3,402) P,Q,HTX,HTY,ACCC,ASSS,AGL
402   FORMAT (2F5.1,5F12.7)
500   CONTINUE
      STOP
      END
```